

INCREASE IN THE BRIGHTNESS OF THE COSMIC RADIO BACKGROUND TOWARD GALAXY CLUSTERS

S. A. Grebenev^{*1} and R. A. Sunyaev^{1,2}

¹Space Research Institute, Russian Academy of Sciences, Profsoyuznaya ul. 84/32, Moscow, 117997 Russia

²Max-Planck-Institut für Astrophysik, Karl-Schwarzschild-Str. 1, Postfach 1317, D-85741 Garching, Germany

Received December 15, 2022; revised April 18, 2023; accepted June 2, 2023

Abstract — We explore the possibility of detecting the excess of the cosmic radio background toward galaxy clusters due to its Compton scattering by electrons of the hot intergalactic gas. When mapping the background fluctuations at frequencies below $\lesssim 800$ MHz, this effect gives rise to a radio source at the location of the cluster. At higher frequencies, where the microwave (relic) radiation dominates in the cosmic background, a “negative” source (a “shadow” on the map of background fluctuations) is observed at the location of the cluster due to the transfer of some of the relic photons upward along the frequency axis upon their scattering (into the range $\nu \gtrsim 217$ GHz; Sunyaev and Zeldovich 1970, 1972). We have computed the spectra of the expected radio background distortions for various parameters of clusters and show that in many cases in the wide frequency range $30 \text{ MHz} \lesssim \nu \lesssim 3 \text{ GHz}$ the measurement of the distortions will be hindered by the intrinsic thermal (bremsstrahlung) radiation from the intergalactic gas and the scattered radio emission from cluster galaxies associated with their past activity, including the synchrotron radiation from ejected relativistic electrons. Below ~ 20 MHz the scattering effect always dominates over the thermal gas radiation due to the general increase in the intensity of the cosmic radio background, but highly accurate measurements at such frequencies become difficult. Below ~ 5 MHz the effect is suppressed by the induced scattering. We have found the frequency ranges that are optimal for searching for and measuring the Compton radio background excess. We show that hot ($kT_e \gtrsim 8$ keV) clusters at high ($z \gtrsim 0.5$) redshifts are most promising for its observation. Because of the strong concentration of the bremsstrahlung to the cluster center, the peripheral observations of the Compton excess must be more preferable than the central ones. Moreover, owing to the thermal radiation of the gas and its concentration to the center, the above-noted transition from the “negative” source on the map of background fluctuations to the “positive” one when moving downward along the frequency axis must occur not gradually but through the stage of a “hybrid source” — the appearance of a bright spot surrounded by a dark ring. This shape of the source in projection is explained by its unusual three-dimensional shape in the form of a narrow radio bremsstrahlung peak rising from the center of a wide deep hole associated with the Compton scattering of the cosmic microwave background. The scattered radiation from a central cluster galaxy active in the past can amplify the effect. An analogous “hybrid source” also appears on the map of background fluctuations near a frequency of 217.5 GHz — when passing from the deficit of the cosmic microwave background to its excess (due to the scattered photons). The unusual shape of the source is again associated with the thermal gas radiation. Simultaneous measurements of the radio bremsstrahlung flux from the gas and the amplitude of the distortions due to the radio and cosmic microwave background scattering will allow the most important cluster parameters to be determined.

DOI: 10.1134/S1063773724700063

Keywords: *cosmic radio background and cosmic microwave background, galaxy clusters, hot intergalactic gas, Compton scattering, Doppler effect, bremsstrahlung and synchrotron radiation.*

INTRODUCTION

The effect of a decrease in the brightness of the microwave background toward galaxy clusters (Sunyaev and Zeldovich 1970, 1972, 1980, 1981; Zeldovich and Sunyaev 1982) is widely used to investigate the properties of clusters and other objects in the early Universe and their evolution. The decrease in brightness is associated with the deficit of cosmic microwave background (CMB) photons relative to the Planck spectrum at frequencies below $\nu_0 \simeq 217$ GHz due to their upward shift along the frequency axis upon Compton scattering by electrons of the hot ($kT_e \sim 3\text{--}15$ keV) intergalactic cluster gas. Here, $h\nu_0 \simeq 3.83 kT_m$, where $T_m = 2.7255$ K is the current CMB temperature. A “shadow” (a “nega-

tive” source) appears on the microwave background map toward a cluster. An excess of photons is formed at frequencies $\nu \gtrsim \nu_0$, and a “positive” source flares up on the background map. The action of the effect is determined by the optical depth of the cluster gas for scattering by electrons $\tau_T = \sigma_T \int N_e(l) dl$, i.e., proportionally to the gas density along the line of sight and not to the square of the density (like the brightness of the thermal gas radiation). Here, σ_T is the Thomson scattering cross section and $N_e(l)$ is the electron density. The amplitude of the effect (the drop in the spectral flux density) does not decrease with distance to the cluster (its redshift z); the shape of the background distortion spectrum does not depend on z either. Owing to these properties, the effect is widely used to determine the parameters of known

^{*}E-mail: grebenev@iki.rssi.ru

clusters and to search for new clusters.

The effect has been successfully observed with the specially built South Pole Telescope (SPT, Carlstrom et al. 2002; Williamson et al. 2011; Bleem et al., 2015, 2020) and Atacama Cosmology Telescope (ACT, Hasselfield et al. 2013; Hilton et al. 2021) as well as a number of other telescopes (Birkinshaw 1999); the Planck satellite (Ade et al. 2014, 2015, 2016) has contributed enormously to the investigation of the effect. Several more specialized instruments and telescopes must join the extensive studies of the effect in the near future (for a review, see Mroczkowski et al. 2019).

The samples of galaxy clusters detected through the effect turn out to be much more representative at high ($z \gtrsim 0.5$) redshifts than the samples of clusters found from X-ray data. Therefore, the dependences of the number of clusters on their mass and z derived from such samples are effectively used to obtain constraints on the parameters of the cosmological models of the Universe (see, e.g., de Haan et al. 2016).

The possibility of observing such an effect in other wavelength ranges is widely discussed. For example, Grebenev and Sunyaev (2019) computed the distortions that appear in the spectrum of the cosmic X-ray and soft gamma-ray background upon its Compton scattering and photoabsorption in the hot gas of galaxy clusters. Sabyr et al. (2022) investigated the distortions that arise upon inverse Compton scattering in the cosmic infrared background spectrum. Cooray (2006) considered the distortions that arise upon scattering by electrons in the 21 cm background profile. Quite recently, Holder and Chluba (2021) and Lee et al. (2022) considered analogous distortions already in the radio background continuum itself.

The cosmic radio background dominates over the CMB at frequencies below ~ 1 GHz. It was discovered in the ARCADE 2 balloon experiment (Fixsen et al. 2011) during highly accurate measurements and was initially discussed as the mysterious ‘‘ARCADE excess’’. The ARCADE 2 measurements were supplemented by the radar observations at low frequencies of 22 and 45 MHz (Maeda et al. 1999; Roger et al. 1999), the LFFSS sky survey at frequencies 40–80 MHz (Dowell and Taylor 2018), and the surveys at 408 MHz (Remazeilles et al. 2015) and 1.4 GHz (Reich et al. 2001). The radio background was shown to have a power-law synchrotron spectrum with a spectral index $\alpha \simeq 0.58 \pm 0.05$ in a wide wavelength range. The nature of the background is still unknown; it is possible to associate no more than 25% of the background radiation with radio galaxies, active galactic nuclei, and other faint compact sources (Seiffert et al. 2011; Condon et al. 2012; Hardcastle et al. 2021). Other reasons for its existence being discussed do not appear convincing either (see Singal et al. 2023). In any case, as it should be for the background, this radio emission is characterized by a high degree of isotropy and homogeneity.

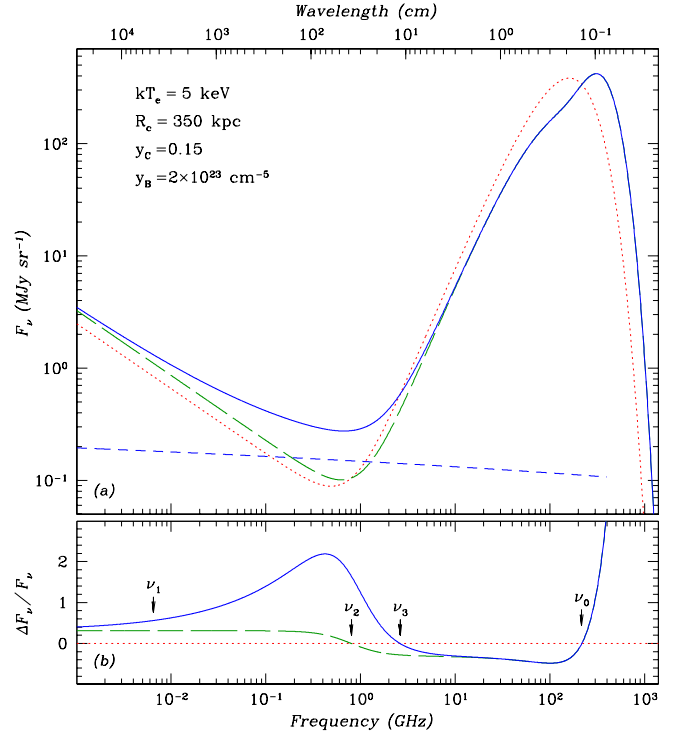


Fig. 1. (a) The radio and microwave background spectrum (red dotted line) and the corresponding distorted spectrum due to the scattering by electrons of the hot gas in a galaxy cluster (long green dashes) and the contribution of the bremsstrahlung from this gas (blue solid line, the spectrum of the bremsstrahlung itself is indicated by the dashed straight line). The demonstration computation for a hypothetical cluster with a uniform density distribution, a radius $R_c = 350$ kpc, a temperature $kT_e = 5$ keV, and Compton, $y_c = 0.15$, and bremsstrahlung, $y_B = 2 \times 10^{23}$ cm $^{-5}$, parameters that actually define the distortion amplitudes (for real clusters y_c and y_B have values that are lower by three orders of magnitude). (b) The relative distortions in the background spectrum toward this cluster (the blue solid curve takes into account the gas bremsstrahlung). The frequencies $\nu_2 \simeq 802$ MHz (of the equality of the Compton radio and microwave background distortions in absolute value), ν_1 and ν_3 (of the equality of the bremsstrahlung flux and the Compton excess in the radio background spectrum or the Compton dip in the CMB spectrum), and $\nu_0 = 217$ GHz (of the transition from the deficit of photons to their excess in this spectrum) are indicated.

The estimates by Holder and Chluba (2021) showed that the Compton scattering of the radio background by electrons of the hot cluster gas increases its brightness at all frequencies (the change in the brightness temperature ΔT reaches ~ 1 mK). Near $\nu_2 \simeq 802$ MHz this increase completely compensates for the above-mentioned decrease in the brightness of the microwave background, i.e., at frequencies $\nu \lesssim \nu_2$ the ‘‘source’’ reappears on the background map toward the cluster instead of the

“shadow”.

In Fig. 1a the background spectrum distorted in the cluster gas that was computed according to Holder and Chluba (2021) is indicated by the long green dashes. The undistorted spectrum (the sum of the cosmic radio and microwave backgrounds) is indicated by the red dotted line. The cluster Compton parameter that defines the amplitude of the spectral distortions is greatly overestimated here, $y_C = \sigma_T \int N_e(l) (kT_e/m_e c^2) dl = 0.15$, but, on the whole, the figure conveys correctly the action of the Compton scattering on the background spectrum. In typical galaxy clusters the parameter y_C has a much lower value. For example, in a cluster with an electron temperature $kT_e = 5$ keV and an optical depth of the gas toward the cloud center $\tau_T = 0.01$ it is $y_C = 1 \times 10^{-4}$.

In this paper we show that the effect predicted by Holder and Chluba (2021) and more rigorously calculated by Lee et al. (2021) is unobservable in most clusters. In the decimeter, meter, and decameter wavelength ranges (frequencies $\nu \lesssim 5$ GHz) the intrinsic bremsstrahlung of the hot intergalactic gas in such clusters exceeds noticeably in flux and completely suppresses the Compton radio and microwave background distortions. This is illustrated by Fig. 1a, in which the background spectrum (long green dashes) including the bremsstrahlung (short blue dashes) is indicated by the blue solid line. The intrinsic gas radiation is seen to dominate in the overall spectrum of the radio emission detected toward the cluster, and only at frequencies below $\nu_1 \simeq 10$ MHz does its flux become equal to the Compton radio background distortions (due to the general increase in the background brightness).

This can be seen even better in Fig. 1b that presents the relative background distortions toward this cluster (with and without the contribution from the intergalactic gas bremsstrahlung). Note that, for demonstration purposes, the gas emission measure toward the center of this hypothetical cluster was greatly overestimated, $y_B = \Sigma_z \int Z^2 N_z(l) N_e(l) dl = 2 \times 10^{23} \text{ cm}^{-5}$ (the summation is over the plasma ions, Z is the nuclear charge of the ion). In reality, it is usually lower by two or three orders of magnitude ($y_B = 1.2 \times 10^{20} \text{ cm}^{-5}$ for the mentioned cluster with $\tau_T = 0.01$). Below in the paper we will calculate the exact values of the above-mentioned frequency ν_1 and the frequency ν_3 at which the gas bremsstrahlung flux completely compensates for the Compton decrease in the CMB brightness for realistic parameters of clusters.

Given the smallness of the parameters y_C and y_B (a factor of 1000 lower than the adopted values) for typical galaxy clusters, Fig. 1b implies that the distortions in the radio background (and centimeter CMB) spectrum considered in the paper are small in absolute value (being fractions of a percent of the background level) and are at the sensitivity limit of modern telescopes. Nevertheless, the rapid development of radio astronomy, as new radio telescopes and radio interferometers are put into opera-

tion, such as GMRT (Venturi et al. 2008), LOFAR (van Haarlem et al. 2013), MeerKAT (Jonas et al. 2016), ALMA/ACA (Di Mascolo 2020), ASKAP (Hotan et al. 2021), SKA (Bacon et al. 2020), CHIME (Amiri et al. 2021), and Tianlei DPA (Wu et al. 2021), promises a noticeable increase in the accuracy and sensitivity of radio measurements and the ability to map the sky at various frequencies with a high angular resolution in the near future. This guarantees the possibility of measuring the subtle effects being discussed in the paper.

THE BACKGROUND SPECTRUM AND ITS DISTORTIONS

Recall the main physical processes that lead to distortions in the spectrum of the background radiation as it interacts with the hot intergalactic gas of a cluster.

Compton scattering. We will consider the interaction of the background radiation with high-temperature electrons in the gas of galaxy clusters by solving the Kompaneets (1957) equation that describes the photon frequency redistribution in the diffusion approximation. The distortions in the CMB spectrum arising in clusters were previously estimated in this way (Sunyaev and Zeldovich 1980; Zeldovich and Sunyaev 1982). The applicability of this equation in the case of an optically thin gas typical for clusters was checked and confirmed by Sunyaev (1980).

The Kompaneets equation is

$$\frac{\partial F_\nu}{\partial \tau_T} = \frac{h\nu}{m_e c^2} \frac{\partial}{\partial \nu} \left[\nu^4 \left(\frac{F_\nu}{\nu^3} + \frac{c^2 F_\nu^2}{2h \nu^6} + \frac{kT_e}{h} \frac{\partial F_\nu}{\partial \nu} \frac{1}{\nu^3} \right) \right] \quad (1)$$

Here F_ν is the spectral intensity of the background radiation. The nonlinear term $\sim F_\nu^2$ on the right-hand side of the equation takes into account the induced scattering, the first term $\sim F_\nu$ is responsible for the recoil effect, it is a factor of $\sim kT_e/h\nu \sim 10^{10}$ smaller than the last (Doppler) term.

Distortions in the CMB spectrum. Neglecting the first two terms, let us substitute the Planck spectrum of the microwave background,

$$B_\nu(\nu) = \frac{2h\nu^3}{c^2} \left[\exp\left(\frac{h\nu}{kT_m}\right) - 1 \right]^{-1},$$

into Eq. (1). We obtain the well-known spectrum of the CMB distortions toward the cluster center

$$\frac{\Delta B_\nu}{B_\nu} = y_C \frac{x e^x}{e^x - 1} \left[x \left(\frac{e^x + 1}{e^x - 1} \right) - 4 \right]. \quad (2)$$

Here, $x = h\nu/kT_m$ and $y_C = \tau_T (kT_e/m_e c^2)$ is the previously introduced Compton parameter that defines the distortion amplitude. In the limit $x \ll 1$ ($\nu \ll 57$ GHz) the relative distortions of the Planck spectrum are negative and do not depend on the frequency,

$$\Delta B_\nu/B_\nu \simeq -2y_C.$$

Distortions in the radio background spectrum. According to Fixsen et al. (2011) and Dowell and Taylor (2018), the intensity of the radio background at our ($z = 0$) epoch is a power-law function of frequency, in terms of the brightness temperature

$$T_R(\nu) = T_* (\nu/\nu_*)^{-2.58 \pm 0.05} \text{ K}, \quad (3)$$

where $\nu_* = 310$ MHz, $T_* = (30.4 \pm 2.1)$ K. Substituting the intensity of the radiation in the form $F_R(\nu) = F_* \nu^{-\alpha}$, where $\alpha = 0.58 \pm 0.05$, into the right-hand side of Eq. (1), we find the spectrum of its relative distortions

$$\Delta F_R/F_R = y_C \alpha(3 + \alpha) \simeq 2.08 y_C. \quad (4)$$

Thus, the relative amplitude of the effect for the radio background is again proportional to the Compton parameter y_C , but, at the same time, it is always positive and does not depend on the frequency ν (Holder and Chluba 2021).

The distortions of the microwave, ΔB_ν , and radio, ΔF_R , background fluxes become equal in absolute value (compensate each other) at a frequency

$$\nu_2 = \nu_* [0.5(3 + \alpha) \alpha T_*/T_m]^{1/(\alpha+2)} \simeq 802 \pm 38 \text{ MHz},$$

which does not depend on the cluster gas parameters (Holder and Chluba 2021).

Distortions due to the induced scattering. The intensity of the radio background at frequencies $\nu \lesssim 2.5$ GHz corresponds to an occupation number $n_\nu(\nu) = F_R(\nu) c^2 / 2h\nu^3 \simeq 2045 (\nu_*/\nu)^{(3+\alpha)} \gtrsim 1$ and, hence, the term in Eq. (1) responsible for the induced Compton scattering cannot be neglected a priori. Retaining this term and substituting again the intensity of the radiation in the form $F_R(\nu) = F_* \nu^{-\alpha}$ into the right-hand side of the equation, we obtain

$$\Delta F_R/F_R = y_C \alpha(3 + \alpha) - \tau_T(1 + \alpha)/m_e F_* \nu^{-(2+\alpha)} \quad (5)$$

The contribution of the induced Compton scattering has a negative sign. This is natural, since it leads to the downward shift of low-frequency photons along the frequency axis (Sunyaev 1970). This contribution becomes equal in absolute value to the Doppler term at $\nu_4 \simeq 1.3 (kT_e/5 \text{ keV})^{-0.39}$ MHz, at lower frequencies the brightness of the radio background turns out to be reduced again.

Bremsstrahlung of the intergalactic gas. The bremsstrahlung surface brightness of an isothermal hot gas in a galaxy cluster toward its center is (Lang 1974)

$$F_B(\nu) = A \frac{\int \Sigma_z (Z^2 N_z) N_e dl}{T_e^{1/2}} g(\nu, T_e) \exp\left(-\frac{h\nu}{kT_e}\right) \quad (6)$$

where the constant $A =$

$$= \frac{8}{3} \left(\frac{2\pi}{3}\right)^{1/2} \frac{e^6 k^{-1/2}}{(m_e c^2)^{3/2}} \simeq 5.4 \times 10^{-39} \frac{\text{erg cm}^3 \text{ K}^{1/2}}{\text{s Hz sr}},$$

and the Gaunt factor

$$g(\nu, T_e) = \frac{\sqrt{3}}{\pi} \ln \Lambda, \text{ where } \Lambda = \frac{4kT_e}{\gamma h\nu} \simeq 4.7 \times 10^{10} \left(\frac{T_e}{\nu}\right)$$

($\gamma \simeq 1.781$, T_e is in K, ν is in Hz). Using the previously introduced bremsstrahlung parameter of the cluster gas (the gas emission measure along the line of sight) y_B , Eq. (6) can be represented as

$$F_B(\nu) = y_B A T_e^{-1/2} g(\nu, T_e) \exp(-h\nu/kT_e). \quad (7)$$

By comparing Eqs. (7) and (4), we can find the frequency ν_1 , at which the radio background distortions ΔF_R and the contribution of the bremsstrahlung F_B become equal. Similarly, by comparing Eqs. (7) and (2), we can find the frequency ν_3 at which the microwave background distortions ΔB_ν in the limit $\nu \ll 57$ GHz become equal in absolute value to the contribution of the bremsstrahlung F_B (they compensate each other). In contrast to the frequency ν_2 , these frequencies are not universal and depend in a certain way on the intergalactic gas temperature and density.

Bremsstrahlung absorption by the intergalactic gas. The bremsstrahlung processes also lead to the absorption of the radio background at low frequencies. The optical depth for this process toward the cluster center is (Lang 1974)

$$\tau_B(\nu) = \frac{F_B(\nu) c^2}{2kT_e \nu^2} = y_B \frac{A c^2}{2k\nu^2} g(\nu, T_e) T_e^{-3/2}, \quad (8)$$

where $F_B(\nu)$ is substituted from Eq. (7). Accordingly, the distortion in the radio background spectrum in addition to the Compton distortions described by Eqs. (4) and (5) that is related to the bremsstrahlung absorption in the intergalactic gas is

$$\Delta F_R/F_R(\nu) = \exp[-\tau_B(\nu)] \simeq 1 - \tau_B(\nu). \quad (9)$$

The bremsstrahlung itself is also absorbed, but to a lesser degree, since its intensity is gained already inside the cluster (along the line of sight).

A MODEL CLUSTER

For clarity and simplicity, we will initially assume the cluster gas to be distributed uniformly and to have the same temperature.

A cluster with a uniform density distribution. Consider a spherically symmetric cloud of hot gas in a cluster with an electron density N_e and temperature T_e that has a radius R_c . The optical depth of such a cluster for Thomson scattering along the line of sight passing through its center is $\tau_T = 2\sigma_T N_e R_c = 2\tau_c$. The electron density in the gas cloud of a typical cluster with an optical depth $\tau_T = 0.01$ and a radius $R_c = 350$ kpc is then $N_e \simeq 7.0 \times 10^{-3} \text{ cm}^{-3}$. The gas mass in the cloud is

$M_g \simeq 3.5 \times 10^{13} (\tau_T / 0.01)(r_c / 350 \text{ kpc})^2 M_\odot$. The total mass M_{500} of the corresponding real (with dark matter) cluster must be at least an order of magnitude greater. This is a moderate-mass cluster like the Coma cluster.

Above and below we assume that hydrogen, helium, and oxygen in the cluster gas have normal cosmic abundances by mass, $X \simeq 0.74$, $Y \simeq 0.24$, and $O \simeq 0.01$ (Cameron 1982), respectively, $N_e \simeq (X + 0.5Y + 0.5O) \rho / m_p \simeq 0.87 \rho / m_p$, the factor appearing in the formula for calculating the bremsstrahlung parameter of the intergalactic gas is $\Sigma Z^2 N_Z \simeq (X + Y + 4O) \rho / m_p \simeq 1.02 \rho / m_p$, and this parameter itself is $y_B = 2 \Sigma Z^2 N_Z N_e R_c \simeq 2.36 N_e^2 R_c$. At temperatures typical for the gas in galaxy clusters, these elements are fully ionized. We will not take into account the heavier elements.

We assume the background radiation to be incident on the cloud isotropically. Accordingly, while computing the spectrum of the radiation emerging from the cloud, we average it over the angles. We assume the radio background, irrespective of its nature (cosmological or associated with unresolved radio galaxies), to be completely formed at high redshifts ($z > z_*$ of the cluster). If this is not the case and some fraction of the radio background is formed at $z < z_*$, then the amplitude of the Compton distortions in its spectrum should be reduced accordingly (by this fraction).

Computation of the background distortions. The blue solid lines in Fig. 2 indicate the contribution of the intergalactic gas bremsstrahlung to the spectrum of the radio and microwave background distortions that should be measured toward the galaxy cluster (the measurements are assumed to be carried out toward the cluster center). The cluster is assumed to be a nearby one, located at a redshift $z \ll 1$. Different lines correspond to different radii R_c of the gas cloud (and, accordingly, different electron densities N_e in it), the Thomson optical depth of the cloud along the line of sight toward the cluster center is $\tau_T = 0.006$, and the electron temperature is $kT_e = 5 \text{ keV}$. The curves also take into account the CMB distortion due to the scattering by electrons of the hot cluster gas (the drop in flux at high frequencies is associated precisely with it, it is indicated separately by the short red dashes). The radio and microwave background distortion due to the inverse Compton scattering by hot-gas electrons is indicated by the long green dashes. The same distortion including the induced scattering is indicated by the short green dashes. The induced scattering shifts the photons downward along the frequency axis, reducing the amplitude of the Compton background distortions at very low frequencies $\nu \lesssim 10 \text{ MHz}$. Yet another effect reducing the distortion amplitude is the bremsstrahlung absorption of radio emission in the hot cluster gas. It is indicated by the green dotted line in addition to the contribution of the induced scattering. In what follows, both these effects will be

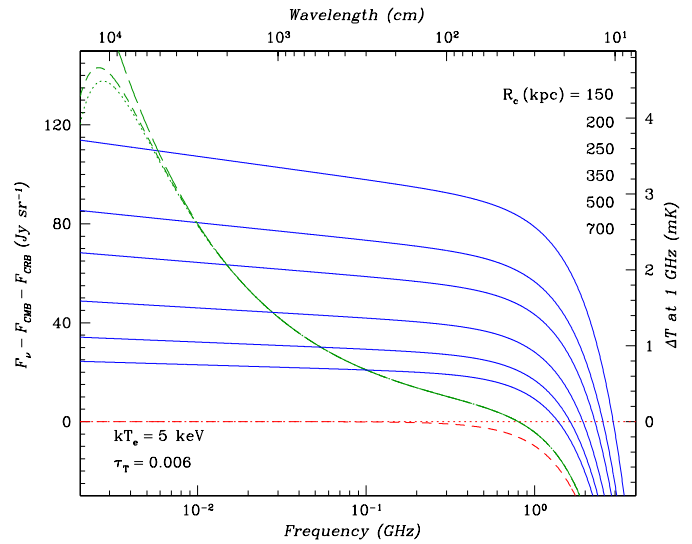


Fig. 2. Comparison of the distortions in the radio background due to its scattering by electrons of the hot cluster gas (long green dashes) and due to the contribution from the bremsstrahlung of this gas (the blue solid lines corresponding to different cluster radii R_c). In both cases, we took into account the CMB distortions due to the scattering by electrons (they are indicated separately by the short red dashes). The short green dashes indicate the decrease in the distortions due to the induced scattering, the green dotted line indicates their decrease also due to the bremsstrahlung absorption of radio emission in the gas. The computation for a nearby ($z \ll 1$) cluster with a uniform density distribution, a temperature $kT_e = 5 \text{ keV}$, and a Thomson optical depth along the line of sight toward its center $\tau_T = 6 \times 10^{-3}$.

ignored, unless stated otherwise.

Bremsstrahlung in the distortion spectrum. It can be seen from Fig. 2, that for the most realistic clusters with radii $R_c = 250 - 350 \text{ kpc}$ the bremsstrahlung dominates over the Compton distortions in the wide frequency range $20 \text{ MHz} \lesssim \nu \lesssim 3.5 \text{ GHz}$. As the compactness of the cluster increases and as the density of its intergalactic gas rises, this range extends to lower frequencies. Obviously, a similar, but less pronounced effect is also to be expected with increasing Thomson optical depth of the cluster τ_T at a constant radius R_c (in this case, the Compton distortions also grow, but not so dramatically as the bremsstrahlung intensity).

The gas bremsstrahlung contributes significantly to the range of high frequencies of the background spectrum, completely or partially compensating for the drop in the CMB flux related to its Compton scattering by high-temperature electrons. To better investigate this question, Fig. 3 presents the distortions in the spectrum $\nu F_\nu(\nu)$ (the intensity multiplied by the frequency) for a cluster with the same gas temperature as that for the cluster in Fig. 2, but with a greater optical depth along

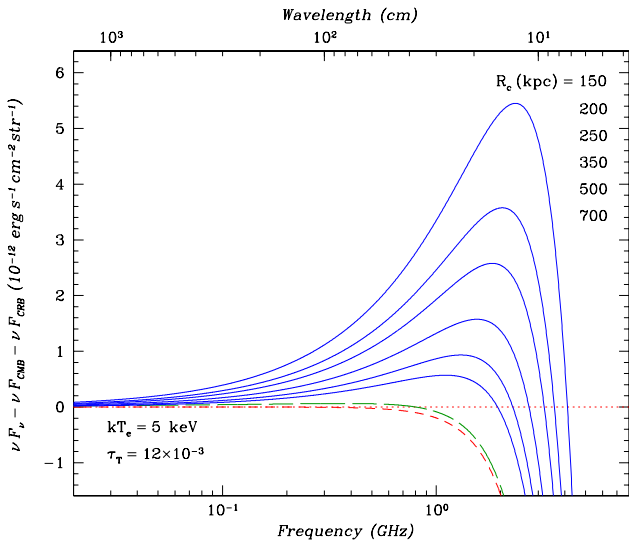


Fig. 3. Same as Fig. 2, but for the distortions in the spectrum $\nu F_\nu(\nu)$, which allows the contribution of the intergalactic gas bremsstrahlung to be investigated better in the centimeter-decimeter wavelength range, where the contribution of the Compton distortions in the CMB spectrum is great. For a gas temperature $kT_e = 5$ keV the bremsstrahlung is seen to compensate for the Compton drop in the flux up to $\lambda \sim 6$ cm ($\nu \sim 5$ GHz). The optical depth of the gas is $\tau_T = 1.2 \times 10^{-2}$ (twice as large as that in Fig. 2).

the line of sight, $\tau_T = 1.2 \times 10^{-2}$. We see that the bremsstrahlung suppresses the drop in CMB brightness up to a frequency $\nu \sim 5$ GHz ($\lambda \sim 6$ cm) and gives rise to a radio source toward the cluster on the maps of background fluctuations at lower frequencies. Without the bremsstrahlung the “shadow” on the background map would be observed up to a frequency $\nu_2 \simeq 802$ MHz. The bremsstrahlung also makes a noticeable contribution at frequencies $\nu \gtrsim 5$ GHz, reducing the expected drop in the CMB flux in the Rayleigh-Jeans part of the spectrum. This process should be taken into account when interpreting the current (for example, VLA and BIMA, Dawson et al. 2002) and planned (the Simons Observatory (SO), Ade et al. 2019; CMB-S4, Abazajian et al. 2019; and CMB-HD, Sehgal et al. 2019) active observations of the effect of a decrease in the CMB brightness at centimeter wavelengths.

Figure 4 shows dependences analogous to those presented in Fig. 2, but for clusters with different parameters of the intergalactic gas cloud: (Fig. 4a) $kT_e = 7$ keV, $\tau_T = 1 \times 10^{-2}$; (Fig. 4b) $kT_e = 15$ keV, $\tau_T = 1.4 \times 10^{-2}$; (Fig. 4c) $kT_e = 3$ keV, $\tau_T = 8 \times 10^{-3}$; and (Fig. 4d) $kT_e = 2$ keV, $\tau_T = 8 \times 10^{-3}$. The parameters of the sample clusters, the temperature of the gas kT_e , and its optical depth for Thomson scattering τ_T , span a wide range of values. It can be seen that in the overall spectrum of the radio background distortions for cold (greatly re-

laxed) clusters the gas bremsstrahlung dominates in a wider frequency range than in the spectrum of hot young clusters. This is because of both the increase in the intensity of the bremsstrahlung itself and the decrease in the amplitude of the distortions in the radio background spectrum upon Compton scattering by electrons linearly dependent on their temperature. The bremsstrahlung of cold clusters with $kT_e = 2 - 3$ keV also extends much farther to high frequency (up to $\nu \sim 7 - 8$ GHz, as can be seen even without constructing a figure analogous to Fig. 3). As noted above, here it competes with the effect of a decrease in the CMB brightness due to the Compton scattering by electrons.

At the same time, the figure suggests that even for the hottest sample clusters with $kT_e = 7 - 15$ keV there exists a noticeable frequency range, $100 \text{ MHz} \lesssim \nu \lesssim 2.5 \text{ GHz}$, in which precisely the intergalactic gas bremsstrahlung must be detected toward the cluster. This is important, since it implies that the transition from the “shadow” on the millimeter-centimeter background map toward the galaxy cluster to the powerful “radio source” on the background map at decimeter and meter wavelengths even in such rich young clusters is associated precisely with the bremsstrahlung of their hot intergalactic gas and not with the Compton distortions of the radio background due to the scattering by gas electrons, as Holder and Chluba (2021) assumed.

Dependence on gas parameters. Obviously, the frequency range $\nu_1 \lesssim \nu \lesssim \nu_3$, where the radio bremsstrahlung of the intergalactic gas dominates in the cluster radiation, serves as the most important characteristic of a galaxy cluster from the viewpoint of its detection on the background maps as a radio source and the identification of the physical process responsible for its appearance. The lower boundary of this range ν_1 is the frequency leftward of which the enhancement of the radio background due to the Compton scattering by electrons of the hot cluster gas exceeds its bremsstrahlung flux. The upper boundary ν_3 is the frequency rightward of which the gas bremsstrahlung flux can no longer compensate for the decrease in the brightness of the microwave background. We explained how to calculate these critical frequencies above in the paragraph following Eq. (7).

Figure 5 presents the results of our attempt to investigate the positions of the frequencies ν_1 and ν_3 (and the width of the interval between them) as a function of the main parameters of the hot cluster gas. Our analysis showed that the electron temperature kT_e and the combination of quantities $\sigma_T y_B / \tau_T$, which is equal to the electron number density in the cluster gas to within a factor of $\simeq 1.18$, are the optimal independent parameters in this problem. This quantity is plotted along the Y axis in the figure. The solid and dotted lines indicate the values of the frequencies ν_1 and ν_3 , respectively. Different curves, but of the same type, correspond to different kT_e . Obviously, the ν_1 and ν_3 curves corresponding to

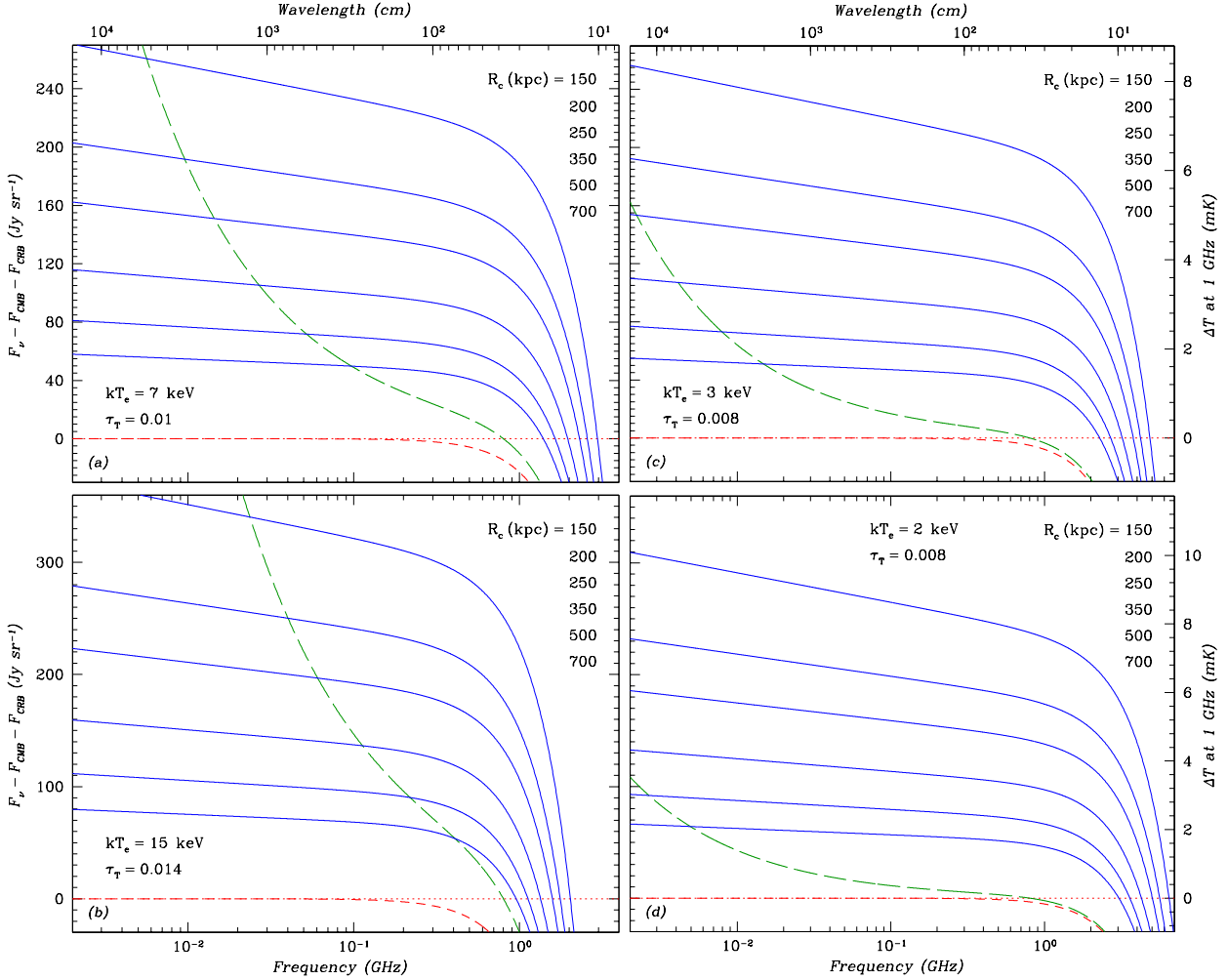


Fig. 4. Same as Fig. 2, but for clusters with the following parameters: (a) $kT_e = 7 \text{ keV}$, $\tau_T = 1 \times 10^{-2}$, (b) $kT_e = 15 \text{ keV}$, $\tau_T = 1.4 \times 10^{-2}$, (c) $kT_e = 3 \text{ keV}$, $\tau_T = 8 \times 10^{-3}$, and (d) $kT_e = 2 \text{ keV}$, $\tau_T = 8 \times 10^{-3}$. The bremsstrahlung (blue solid lines) dominates in a wider spectral range for cold, greatly relaxed clusters. At the same time, it completely compensates for the drop in CMB brightness up to frequencies of 5–8 GHz ($\lambda \simeq 4 - 6 \text{ cm}$) and weakens it at higher frequencies. Although the distortions in the radio background spectrum become stronger for hot young clusters with a large optical depth, they become equal to the bremsstrahlung only at very low frequencies $\nu \lesssim 20 \text{ MHz}$ ($\lambda \gtrsim 15 \text{ m}$).

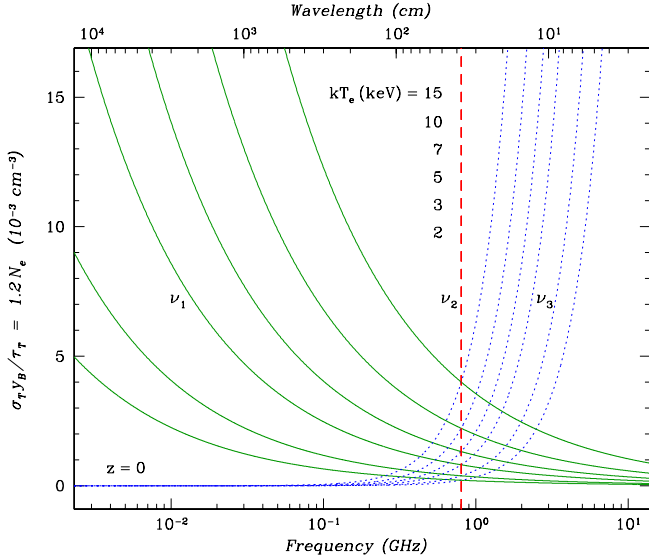


Fig. 5. The boundary frequency ν_1 above which the bremsstrahlung flux from the intergalactic cluster gas dominates over the Compton enhancement of the radio background in the overall distortion spectrum (green solid curves) and frequency ν_3 below which the bremsstrahlung dominates in absolute value over the Compton attenuation of the CMB flux (blue dotted curves). The curves for different gas temperatures in the cluster are shown. The vertical red dashed line indicates the frequency ν_2 at which the Compton distortions of the radio background and the CMB become equal. The positions of the frequencies ν_1 and ν_3 are given as a function of intergalactic gas temperature kT_e and density N_e (to be more precise, $\sigma_T y_B / y_C [kT_e / m_e c^2] \simeq 1.18 N_e$).

the same temperature intersect at the frequency ν_2 for which in the absence of bremsstrahlung the Compton distortions in the synchrotron (power-law) radio background and the Planck microwave background spectrum become equal in absolute value.

Figure 5 suggests that the region of frequencies with the dominant contribution of the bremsstrahlung must be present in the background distortion spectra toward all typical nearby clusters. However, it narrows noticeably for very hot and anomalously sparse clusters. The critical value of $(\sigma_T y_B / \tau_T)_{\min} \simeq 1.18 N_{e,\min}$ at which this region should have collapsed ($\nu_1 \rightarrow \nu_2$, $\nu_3 \rightarrow \nu_2$) is shown in Fig. 6 as a function of temperature kT_e and cluster redshift z (see below). It can be seen that the minimum gas density at which the bremsstrahlung region still exists in the distortion spectrum increases with gas temperature.

For clarity, on the right Y axis of Fig. 6 we show what the cluster radius R_c with the critical electron density must be. The Thomson optical depth toward the cluster center is fixed at a comparatively low value of $\tau_T = 0.006$ (barely sufficient for the formation of a Compton distortion in the radio background accessible to observa-

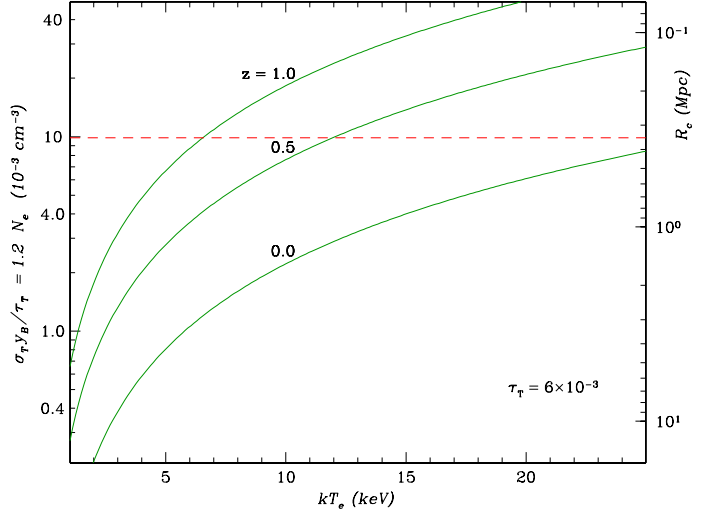


Fig. 6. The minimum electron density $N_{e,\min}$ (to be more precise, $\sigma_T y_B / \tau_T \simeq 1.18 N_{e,\min}$) of the hot intergalactic gas needed for the frequency range with the dominant contribution of the bremsstrahlung to exist in the spectrum of the radio background distortions toward the cluster. The density is higher for distant ($z > 0$) clusters. The radius R_c of a cluster with the critical density and a Thomson optical depth toward the center $\tau_T = 6 \times 10^{-3}$ is plotted on the Y axis on the right. The dashed line marks a typical cluster radius $R_c \simeq 350$ kpc.

tions). Nevertheless, even in the case of the hottest (but nearby, $z \simeq 0$) clusters in this figure, with $kT_e \gtrsim 20$ keV, the gas bremsstrahlung does not contribute to the radio flux only when their radius R_c exceeds noticeably the actually observed cluster sizes ($R_c \gtrsim 500$ kpc).

Dependence on redshift z . The change in the spectrum of the microwave background with redshift is completely determined by the dependence of its temperature on z : $T_m(z) = T_m(1+z)$. The radio background spectrum (Eq. [3]) depends on z in a more complicated way: $F_R(z) = F_0 (\nu/\nu_0)^{-\alpha} (1+z)^{3-\alpha}$ (Zeldovich and Novikov 1975), and only under the assumption that the power-law shape of the spectrum does not change with redshift. We are interested in the background spectrum at the present epoch, and, as has already been noted, it was measured with a high accuracy. Its dependence on z does not change the distortions observed at our epoch that arise in it when interacting with the intergalactic gas of galaxy clusters, no matter how far they are.

The radio bremsstrahlung spectrum of this gas, whose brightness changes as $F_B(z=0) = F_B(z)/(1+z)^3$ when observing distant clusters (the gas temperature after its measurement was assumed to have been corrected for z , i.e., reduced to the cluster frame), is a different matter. Since the radio bremsstrahlung spectrum itself depends weakly on the frequency, $F_B \sim \nu^{-0.04}$, the change with

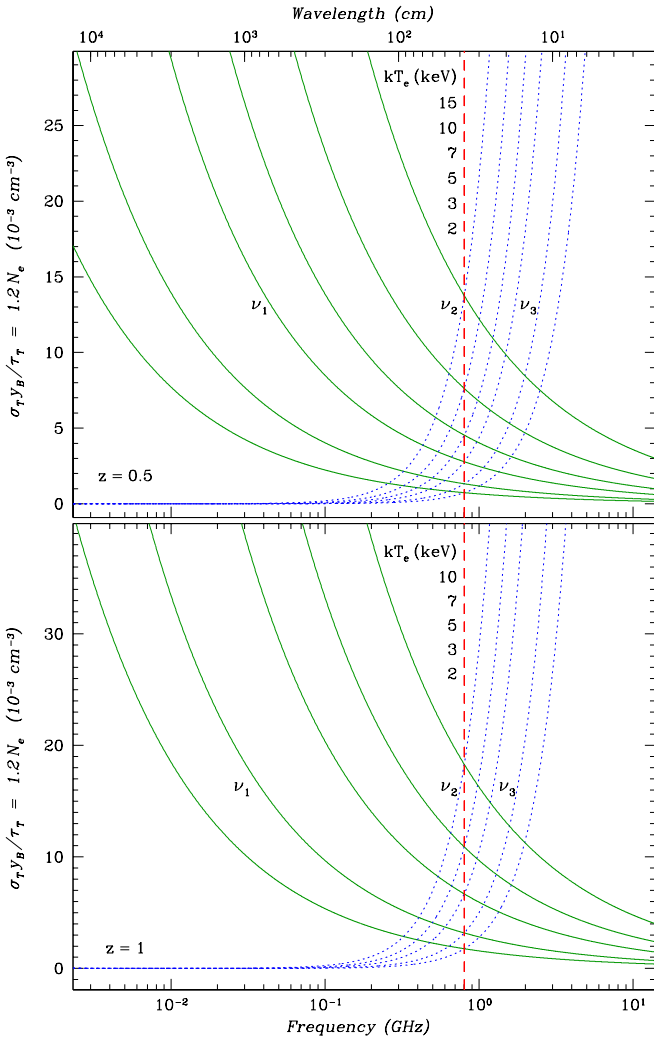


Fig. 7. Same as Fig. 5, but for distant clusters at redshifts $z = 0.5$ and 1 . Because of the drop in bremsstrahlung brightness with z , the frequency range in which the bremsstrahlung dominates in the background distortion spectrum toward the cluster narrows noticeably.

z is reduced to a drop in the flux from distant clusters by the same factor at all frequencies $(1+z)^3$. Figure 7 shows how the frequency range $\nu_1 < \nu < \nu_3$ with the dominant bremsstrahlung in the distortion spectrum narrows when observing clusters at redshifts $z = 0.5$ and 1 . This figure is analogous to Fig. 5, which presents the same frequency range $\nu_1 < \nu < \nu_3$, but typical for local ($z \ll 1$) clusters.

Figure 6 presents the curves of the critical density $N_{e,\min}$ at which the frequency range with the dominant bremsstrahlung is still absent in the distortion spectrum for two such distant ($z = 0.5$ and 1) clusters. It can be seen that as the redshift of the cluster increases, the observed intensity of its radio bremsstrahlung drops rapidly; accordingly, it may not be detected at all against the Compton radio background distortions even in the case when it has a lower temperature and a higher gas

density than do similar local clusters. The constraints on the critical cluster radius also weakens.

REAL CLUSTERS

Above we have assumed that the radio flux is measured toward the cluster center and with a good angular resolution (compared to the angular size of the cluster). Obviously, the peripheral observations of the gas in clusters with a uniform density distribution are less preferable, since in this case both the gas bremsstrahlung flux and the amplitude of the radio background distortions due to the scattering decrease equally (proportionally to l — the cluster size along the line of sight). The situation is different if the peripheral observations are carried out in the case of a real cluster with a density that falls off slowly with radius. Since the amplitude of the background distortions due to the scattering and the bremsstrahlung intensity are proportional to N_e and N_e^2 , respectively, the contribution of the bremsstrahlung to the observed radio background excess decreases to the cluster edge faster than does the contribution of the scattering (Zeldovich and Sunyaev 1982).

Nonuniform density distribution. Let us illustrate this effect using a cluster characterized by a β gas density distribution along the radius (Cavaliere and Fusco-Femiano 1976),

$$N_e = N_c \left(1 + \frac{R^2}{R_c^2} \right)^{-3\beta/2}, \quad (10)$$

with a central electron density N_c and a parameter $\beta \simeq 2/3$ that agrees well with the observed X-ray brightness distribution of many galaxy clusters (Jones and Forman 1984; Arnaud 2009) as an example. For such a cluster the bremsstrahlung parameter (emission measure) of the intergalactic gas $y_B(\rho) = 2 \int_0^\infty \Sigma Z^2 N_Z(R) N_e(R) dl$, which defines the intensity of its thermal radiation along the line of sight at an impact parameter ρ from the direction toward the center, is

$$y_B(\rho) = 0.59 \pi \left(1 + \frac{\rho^2}{R_c^2} \right)^{-3/2} N_c^2 R_c. \quad (11)$$

The radius R , the impact parameter ρ , and the distance along the line of sight l are related by the expression $R^2 = \rho^2 + l^2$.

The Thomson optical depth of the gas along the line of sight $\tau_T(\rho) = 2\sigma_T \int_0^\infty N_e(R) dl$, which defines the amplitude of the spectral distortions due to the scattering, is

$$\tau_T(\rho) = \pi \left(1 + \frac{\rho^2}{R_c^2} \right)^{-1/2} \sigma_T N_c R_c. \quad (12)$$

Figure 8 presents the distortions in the radio and microwave background spectrum in such a cluster expected due to the Compton scattering by electrons (green dashes) and the contribution of the thermal

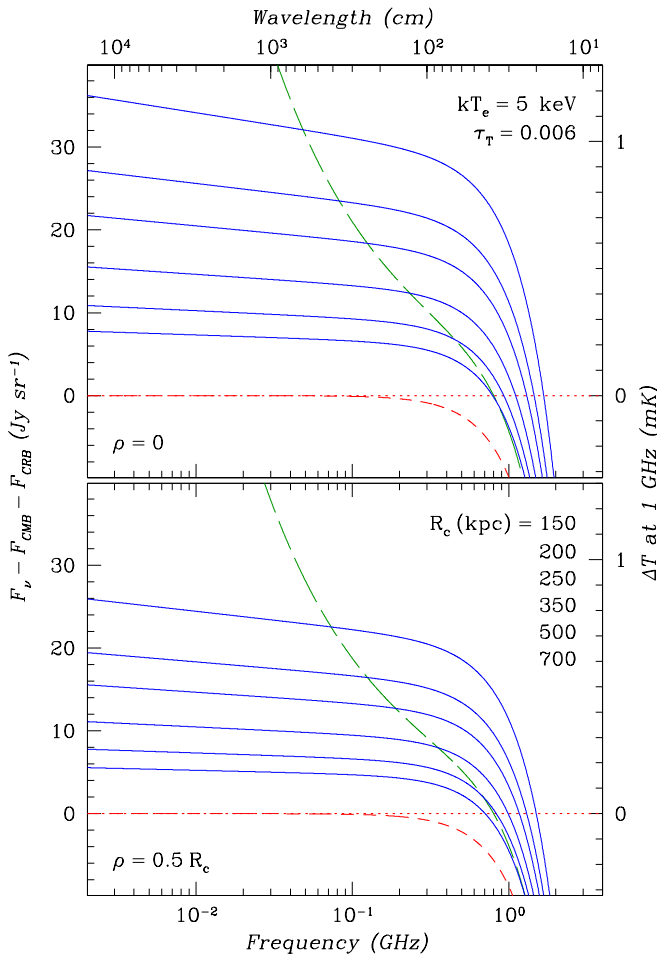


Fig. 8. Same as Fig. 2, but for a cluster with a β gas density distribution ($\beta = 2/3$). The Thomson optical depth toward the cluster center is $\tau_T = 6 \times 10^{-3}$, the gas is isothermal with $kT_e = 5$ keV, the cluster is a nearby one ($z \ll 1$). The contribution of the bremsstrahlung is indicated by the blue solid lines for different cluster core radii R_c . The central (impact parameter $\rho = 0$, the upper panel) and peripheral ($\rho = 0.5 R_c$, the lower panel) observations are considered.

bremsstrahlung (blue solid lines) at two impact parameters, $\rho = 0$ and $0.5 R_c$. The gas parameters, the radial Thomson optical depth $\tau_c = 3 \times 10^{-3}$ and the electron temperature $kT_e = 5$ keV, were chosen to be the same as those for a cluster with a uniform density distribution in Fig. 2. Various values of the cluster core radius R_c were considered. It can be seen that the Compton background distortions toward the cluster center ($\rho = 0$) in Figs. 2 and 8 are indeed the same because of the equality of the optical depths. However, the intensity of the thermal radiation from the gas of a real cluster is a factor of π lower than the intensity of the radiation from a cluster with a uniform gas density distribution.

This result is easy to explain: although the gas in a real cluster is more strongly concentrated to the center, its density is slightly lower (by a factor of $\pi/2 \simeq 1.57$)

than the gas density in a homogeneous cluster with the same core radius R_c and optical depth τ_T . A sizeable fraction of the optical depth is gained at large radii $R > R_c$. Similarly, the cluster gas mass

$$M_g(< R) = 4.6 \left(\frac{\tau_T m_p}{\sigma_T} \right) R_c^2 \left[\frac{R}{R_c} - \arctg \left(\frac{R}{R_c} \right) \right]$$

within the radius $R = R_c$ is comparatively small, $M_g(< R_c) \simeq 4.8 \times 10^{12} M_\odot$, but it increases rapidly with R , reaching $M_g(< 2 R_c) \simeq 2 \times 10^{13} M_\odot$ at $R = 2 R_c$, which is already close to the gas mass in a homogeneous cluster ($\simeq 2.1 \times 10^{13} M_\odot$ at $\tau_T = 0.06$).

The intensity of the thermal radiation from the gas of a real cluster decreases still more dramatically when it is observed even at a small ($\rho \sim 0.5 R_c$, Fig. 8, lower panel) distance from the direction toward the center. In the case of such peripheral observations, the action of the Compton scattering effect also weakens with regard to both radio (green dashes) and microwave (short red dashes) backgrounds (and equally, so that the frequency ν_2 does not change), but this occurs much more slowly. Therefore, the peripheral observations of real clusters turn out to be advantageous from the viewpoint of detecting the scattering effect.

Figure 9, which is also based on Eqs. (11) and (12), shows how the brightness of the cosmic radio background at various frequencies changes with impact parameter ρ . We again considered a nearby cluster with a β density distribution, but with a higher temperature $kT_e = 7$ keV and an optical depth $\tau_T = 0.01$ of the gas (as in Fig. 4a). The cluster core radius is $R_c = 350$ kpc. It can be seen that the thermal radiation of the gas toward the cluster center dominates in the increase in radio brightness at frequencies $\gtrsim 200$ MHz, but even at a small ($\rho \gtrsim 2 R_c$) distance from this direction a major contribution to the increase in the brightness of the radio background is made by its scattering by electrons at all of the frequencies considered. As the frequency increases, the region with the dominant thermal radiation slightly expands.

Note that in Fig. 9 (its upper panel) (at frequencies $\lesssim 700$ MHz) the thermal and scattered radio emissions form a positive source at any ρ . Positive radiation is observed on the lower panel only at small $\rho \lesssim R_c$ and frequencies $\nu \lesssim 1200$ MHz. The point is that when calculating the distortions, in addition to the Compton scattering of the radio emission, we took into account the scattering of the CMB by electrons, which leads to a decrease in background brightness in the central cluster regions (Sunyaev and Zeldovich 1970, 1972; indicated by the red solid lines). As mentioned above, the Compton distortions of the microwave and radio emissions become equal in absolute value (compensate each other) at $\nu_2 \simeq 802$ MHz, and this can be seen on the upper panel of Fig. 9. At higher frequencies the observed background excess is associated exclusively with the thermal gas radiation.

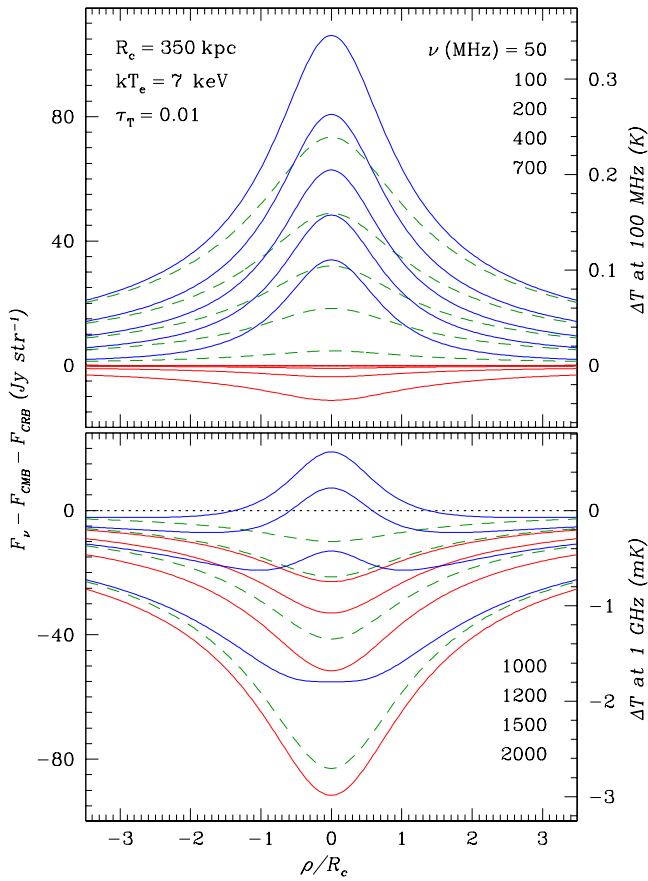


Fig. 9. Comparison of the distortions in the radio background due to its scattering by electrons of the hot cluster gas (green dashes) and the bremsstrahlung of this gas (blue solid lines) at various frequencies as a function of the impact parameter ρ/R_c from the direction toward the cluster center. The CMB distortions due to the scattering by gas electrons (red solid lines) were also taken into account. The computation for a nearby ($z \ll 1$) cluster with a β density distribution ($\beta = 2/3$), a core radius $R_c = 350$ kpc, a temperature $kT_e = 7$ keV, and a Thomson optical depth toward the center $\tau_T = 1 \times 10^{-2}$ (see Fig. 4a).

It can be seen from Fig. 9 that (1) the decrease in the brightness of the microwave background toward the cluster center begins to be suppressed by the intrinsic thermal radiation of the gas starting already at frequencies $\nu \sim 2.0$ GHz, being completely compensated near $\nu \sim 1.3$ GHz, (2) even at small distances from the center $\rho \gtrsim R_c$ the reduced background is retained up to frequencies ~ 800 MHz, and (3) at frequencies $\nu \lesssim 300$ MHz the decrease in CMB brightness disappears completely irrespective of the Compton scattering of the radio emission or the contribution of the thermal gas radiation. This is because of the fast natural (Rayleigh-Jeans) drop in the CMB flux when moving downward along the frequency axis and the equally fast rise in the flux of the cosmic radio background.

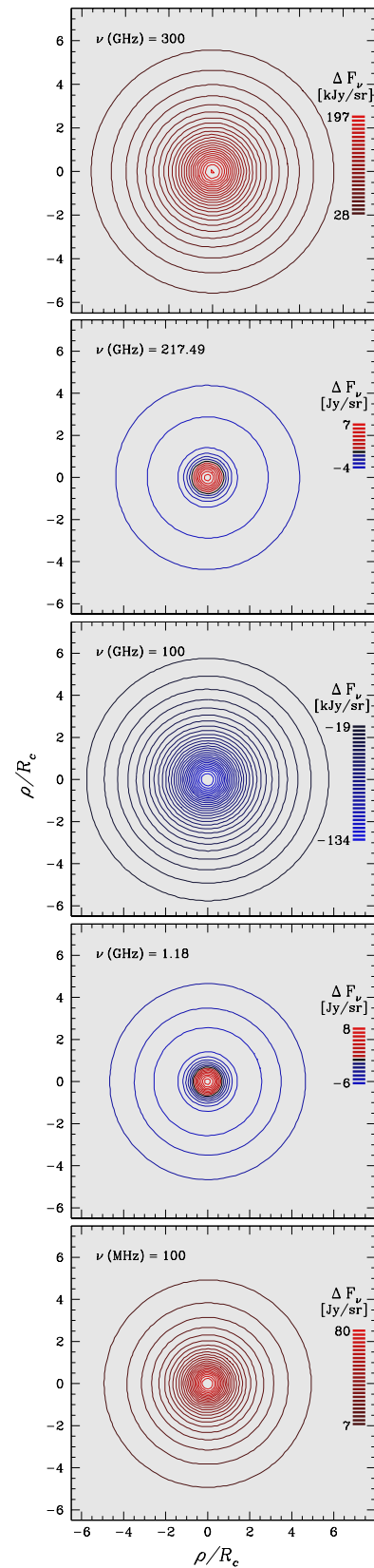


Fig. 10. Map of cosmic microwave and radio background distortions toward the same galaxy cluster as that in Fig. 9 at various frequencies (the blue and red lines indicate the “negative” and “positive” deviations, respectively). The outer contours (at distances $\rho \gtrsim 6 R_c$) are not shown.

A source of hybrid shape at the location of the cluster.

Obviously, the downward transition in frequency in the spectrum of the background distortions measured toward a galaxy cluster from the region of decreased brightness (CMB) to the region of increased brightness (radio emission) must be accompanied by a change in the image of the source on the maps of background fluctuations. Figure 9 (its lower panel) predicts that in the frequency range $1.0 \text{ GHz} \lesssim \nu \lesssim 1.2 \text{ GHz}$ the cluster image must take a highly unusual form — a bright source at the center (excess bremsstrahlung) surrounded by a ring-like shadow region (a region of CMB deficit). This can be seen even better from Fig. 10 that shows the modeled maps of microwave and radio background distortions at various frequencies toward a nearby galaxy cluster with the same gas parameters as those used in constructing Fig. 9. The unperturbed background was subtracted.

An unusual (hybrid) source is seen on the map for $\nu = 1.18 \text{ GHz}$. At higher frequencies ($\nu = 100 \text{ GHz}$) the central source disappears and the shadow region expands to a circle with a radius exceeding noticeably the cluster core radius.¹ The source on the map of background fluctuations at the location of the cluster becomes “negative” — a “hole” in the background. It is known to turn again into an ordinary “positive” source at frequencies above $\nu_0 \simeq 217.5 \text{ GHz}$ ($\lambda \simeq 1.37 \text{ mm}$, Sunyaev and Zeldovich 1980, 1982) due to the lower-frequency CMB photons thrown into this region by the inverse Compton scattering. This is illustrated by the map for a frequency of 300 GHz . At the other edge of the spectrum, at frequencies $\lesssim 800 \text{ MHz}$, the hybrid source at the location of the cluster described above also turns into a completely “positive” source primarily due to the Rayleigh-Jeans decrease in the CMB flux and, accordingly, in the absolute depth of the Compton “hole” forming in it, but also due to the excess associated with the Compton scattering of the growing radio background and the contribution of the intergalactic gas bremsstrahlung. In Fig. 10 the transition to the “positive” source is illustrated by the lower map computed for $\nu = 100 \text{ MHz}$.

The appearance of a source with a hybrid shape on the map of background fluctuations is explained by the strong concentration of the thermal (bremsstrahlung) radiation from the intergalactic gas to the cluster center. The Compton CMB distortions forming the “shadow” (“hole”) on the map are characterized by a larger spatial scale, which is explained by their weaker (linear) dependence on the hot-gas electron density.

The change in the shape of the source on the maps of background fluctuations for this cluster during the transition near $\nu \sim 1.1 \text{ GHz}$ from the completely “negative” source to the completely “positive” one is shown

in more detail in Fig. 11. It can be seen that the transition occurs slowly, the hybrid source is observed in a wide frequency range, $1.0 \text{ GHz} \lesssim \nu \lesssim 1.25 \text{ GHz}$, well above the frequency $\nu_2 \simeq 802 \text{ MHz}$ of the mutual compensation of the Compton CMB and radio background distortions. The thermal radiation of the hot gas is also seen at frequencies $1.4 \text{ GHz} \lesssim \nu \lesssim 1.8 \text{ GHz}$ — it forms a central narrow peak inside the hole produced by the inverse Compton scattering of the CMB. The hole at these frequencies simply turns out to be deeper, and the thermal radiation peak cannot rise above its edge and manifest itself as a clear “positive” central source. In fact, at these frequencies a hybrid source, but in a latent form, is also observed at the location of the cluster. Note also the map for $\nu = 900 \text{ MHz}$. The source at the location of the cluster on this map is largely associated with the thermal radiation of the intergalactic gas and has a noticeably smaller width than on other maps, where it is formed primarily due to the Compton scattering of the background. At $\nu = 900 \text{ MHz}$ the distortions due to the scattering of the radio and cosmic microwave backgrounds compensate each other almost completely.

Surprisingly, when passing through $\nu_0 \simeq 217.5 \text{ GHz}$, the source at the location of the cluster in Fig. 10 also takes a hybrid shape. Previously, it has always been thought that the “negative” source at the location of the cluster near this frequency simply disappears to subsequently appear at higher frequencies as a completely “positive” one. The frequency $\nu_0 = 3.8300 kT_m \simeq 217.5065 \text{ GHz}$ is calculated from the condition for the right-hand side of Eq. (2), which describes the change in the CMB spectrum upon Compton scattering, to become zero. The hybrid shape of the source is again associated with the intergalactic gas bremsstrahlung concentrated to the cluster center that becomes noticeable due to the attenuation of the Compton CMB distortions near this frequency. Note that the intensity levels on the maps in Fig. 10 for $\nu = 100$ and 300 GHz (immediately below and above ν_0) are given in kJy/sr , whereas those on the map with $\nu = 217.47 \text{ GHz}$ and the remaining maps are given in Jy/sr . The change in the shape of the source at the location of the cluster on the maps of CMB fluctuations when passing through ν_0 is studied in detail in Grebenev and Sunyaev (2024).

The detection of a hybrid source toward a galaxy cluster in both CMB and radio background can be interesting not only as a demonstration (and confirmation) of an elegant physical effect. It may turn out to be important for a more accurate separation of the radio background distortions due to the Compton scattering and the contribution from the radio bremsstrahlung of the cluster gas. One can attempt to estimate the radio bremsstrahlung flux from X-ray cluster observations, but the accuracy of such estimates depends critically on the reliability of the determination of the gas temperature kT_e . Direct measurements of the thermal radio flux from the intergalactic gas may turn out to be more promising

¹The shadow region in the hybrid source actually extends also noticeably farther along the radius than follows from the figure, but in this source it has a smaller depth. The low-intensity levels corresponding to the far wings of the source (large impact parameters $\rho/R_c \gtrsim 6$) are simply not shown on these panels.

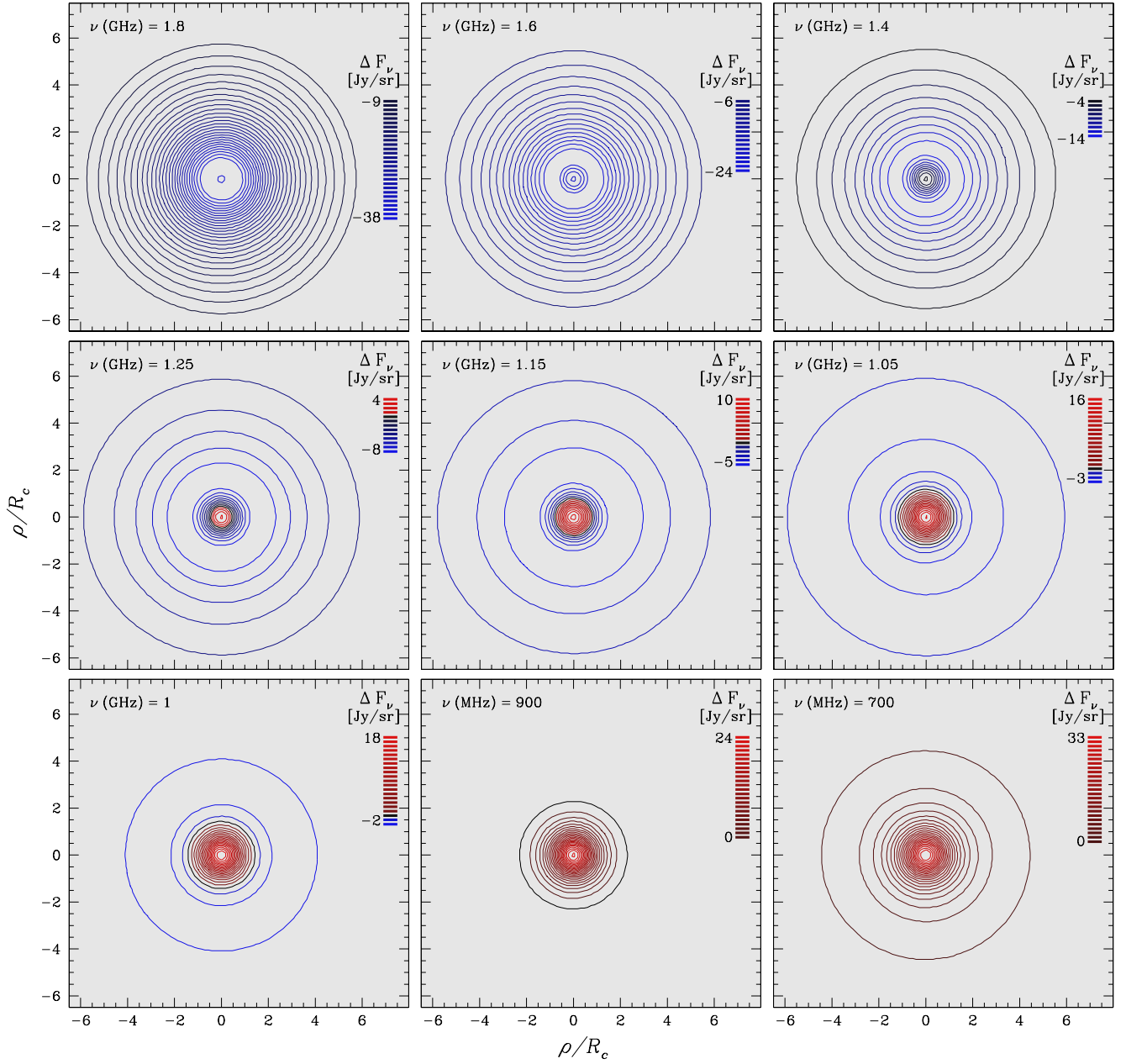


Fig. 11. Evolution of the map of radio and microwave background distortions toward a galaxy cluster during the transition between the regimes of decreased and increased brightness (the blue and red lines indicate the “negative” and “positive” background deviations, respectively). The distortions are caused by the scattering by electrons, but the appearance of a hybrid source (a bright spot surrounded by a dark ring) and a compact “positive” source on the map for $\nu = 900$ MHz is largely associated with the thermal radiation of the hot cluster gas. The outer ($\rho \gtrsim 6 R_c$) contours on the maps with $\nu \leq 1.0$ GHz are not shown. The computation for a nearby ($z \ll 1$) cluster with a β density distribution ($\beta = 2/3$) and the same parameters as those for the cluster in Figs. 9 and 10.

Table 1. Parameters of the individual clusters selected to assess the possibility of measuring the effect of radio background scattering by electrons of their hot intergalactic gas

| Cluster name ^a | | z^b | R_c^c | θ_c^c | kT_e | N_c^d | M_g^e | τ_T^f |
|---------------------------|---------------|-------|---------|--------------|--------|---------|---------|------------|
| main | alternative | | | | | | | |
| 1 | 2 | 3 | 4 | 5 | 6 | 7 | 8 | 9 |
| AT J0102-4915 | El Cordo | 0.870 | 270 | 0.75 | 14.5 | 8.9 | 2.2 | 15.2 |
| A 426 | Perseus | 0.018 | 280 | 12.8 | 6.0 | 4.6 | 2.0 | 8.3 |
| ST J0615-5746 | P G266.6-27.3 | 0.972 | 230 | 0.63 | 14.2 | 7.2 | 1.12 | 10.5 |
| 1E0657-558 | Bullet | 0.296 | 170 | 0.73 | 12.4 | 12.3 | 2.01 | 13.3 |
| A 1656 | Coma | 0.023 | 290 | 10.5 | 6.9 | 2.9 | 1.0 | 5.6 |
| Virgo | | 0.004 | 310 | 62.5 | 2.4 | 2.7 | 1.5 | 5.3 |
| A 1991 | | 0.059 | 60 | 0.90 | 2.3 | 6.4 | 0.1 | 3.5 |
| ST J2106-5844 | | 1.132 | 200 | 0.54 | 9.4 | 11.5 | 1.17 | 14.6 |
| ST J2248-4431 | AS 1063 | 0.348 | 370 | 1.4 | 11.5 | 2.9 | 1.95 | 7.0 |
| ST J2344-4243 | Phoenix | 0.596 | 290 | 0.88 | 14.9 | 4.8 | 1.48 | 8.8 |

^a A – Abell, ST – SPT-CL, AT – ACT-CL, P – PLCK.

^b The cluster redshift.

^c The core radius in the model of a β density distribution and its angular size.

^d The gas density at the cluster center, 10^{-3} cm^{-3} .

^e The gas mass in the cluster.

^f The Thomson optical depth along the line of sight passing through the cluster center.

and reliable.

Individual clusters. Let us assess the possibility of detecting the distortions of the radio background associated with its scattering by intergalactic gas electrons toward several known galaxy clusters. We will assume the gas to be isothermal and to have a β density distribution with $\beta = 2/3$. We will make our estimates for rich clusters that manifest themselves by strong microwave background distortions from the sample used in Grebenev and Sunyaev (2019). Table 1 gives the main characteristics of the intergalactic gas (its temperature and central density, other parameters of the β -model) and the clusters themselves (redshift z).

The long green dashes in Fig. 12 indicate the expected relative (in %) Compton distortions in the radio and microwave background spectrum for several clusters from this sample. The observations are assumed to be carried out toward the cluster center (the left panel of Fig. 12) or at an impact parameter $\rho = 0.8 R_c$ relative to the center (its right panel). The unperturbed background level is marked by the short black dashes. The red dotted lines indicate the contribution from the effect of a decrease in brightness due to the scattering of only the CMB to the distortion spectrum. It can be seen that the relative Compton distortions do not depend on the frequency in the case of both the radio background and the CMB (in complete agreement with the predictions of Eqs. [2] and [4]). Moreover, they are almost equal in magnitude, but have different signs. The blue solid lines indicate the background distortions including the

intrinsic bremsstrahlung of the hot cluster gas.

Figure 12 shows that the scattering of the radio emission in a number of nearby clusters leads either to very small (the Coma and Perseus clusters) or negligible (the Virgo and A 1991 clusters) background distortions. The low temperatures ($kT_e \sim 2.5 - 6.9$ keV) and quite moderate optical depths ($\tau_T \lesssim 8 \times 10^{-3}$) of the gas contained in them have an effect. At the same time, the radio bremsstrahlung of these nearby ($z \lesssim 0.06$) clusters is fairly strong. This manifests itself particularly clearly on the left panel of the figure, in the observations toward the cluster center. The detectability of the radio background distortions in the first two clusters can be increased by integrating the radio signal over their fairly large apparent area (the angular size of these clusters is specified in Fig. 12 on the left). As has already been mentioned (and will be shown below), the contribution of the scattered radiation to the overall spectrum of the radio background distortions increases compared to the contribution of the bremsstrahlung (due to the strong concentration of the latter to the cluster center). Another possibility is to observe the distortions at an appreciable impact parameter $\rho \sim R_c$ from the cluster center, as shown on the right panel of Fig. 12. It can be seen that even at an impact parameter $\rho = 0.8 R_c$ the bremsstrahlung intensity is a factor of ~ 2.1 lower than the intensity toward the cluster center, with the amplitude of the Compton background distortions changing not too dramatically ($< 30\%$).

Nevertheless, it is obvious that to detect the Compton distortions, it is much more promising to observe very

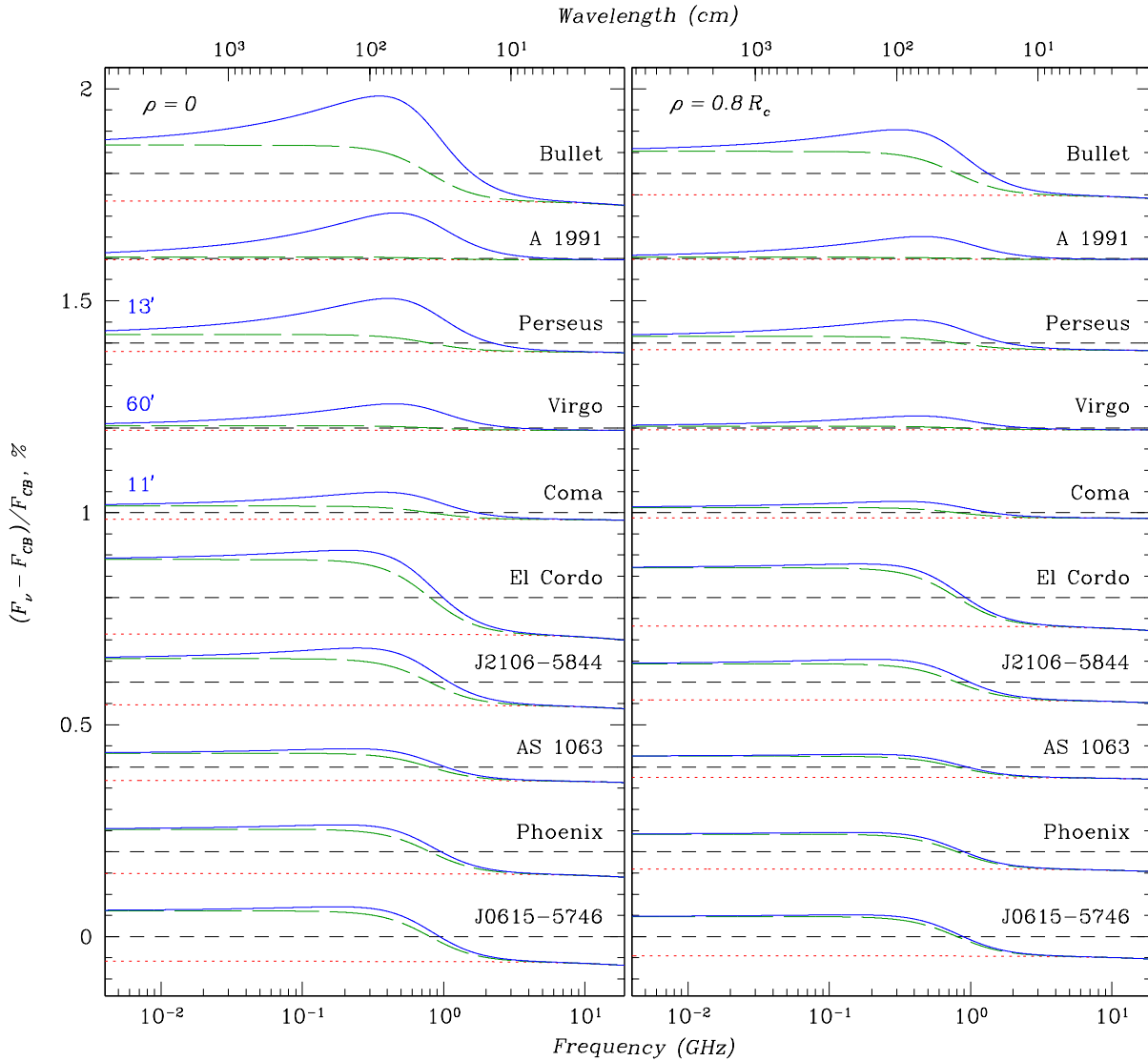


Fig. 12. The relative (in %) distortions in the spectrum of the cosmic radio and microwave background expected due to its scattering by hot-gas electrons in several known galaxy clusters (long green dashes). The blue lines also take into account the thermal (bremsstrahlung) radiation of the gas. The decrease in CMB brightness due to its scattering by electrons is indicated by the red dotted lines. The distortions observed toward the cluster center (*left*) and at an impact parameter close to the cluster core radius $\rho = 0.8 R_c$ (*right*). The gas is assumed to be isothermal and to have a β density distribution ($\beta = 2/3$), the cluster parameters are given in Table 1.

hot ($kT_e \gtrsim 12$ keV), optically thick ($\tau_T \gtrsim 8 \times 10^{-3}$), distant ($z \gtrsim 0.35$) clusters: El Cordo, Phoenix, AS 1063, ST J0615-5746 and ST J2106-5844. The Compton background distortions in such clusters can reach $\sim 0.1\%$; the main obstacle for their measurement in the form of hot-gas bremsstrahlung weakens noticeably due to the great distance of the clusters (high z). The Bullet cluster, one of the hottest and optically thickest clusters, but, at the same time, with powerful thermal gas radiation, is an exception. This is partly because of its moderate redshift $z \simeq 0.3$, and partly because of its unusual compactness, $R_c \simeq 170$ kpc, and, as a consequence, the enhanced density of its gas $N_c \simeq 1.23 \times 10^{-2} \text{ cm}^{-3}$. Even in the de-

cameter wavelength range and in the case of peripheral observations, it will be difficult to detect the Compton background distortions toward this cluster.

Observations of unresolved clusters. The angular size of many distant clusters is too small to perform their peripheral observations. In this case, their entire radio flux or the integrated flux from the wide central part of the cluster is measured.

Take a cluster with a β hot-gas density distribution and a core radius $R_c = 350$ kpc. Consider two cases where the cluster is located at $z = 0.11$ or 0.3 . The

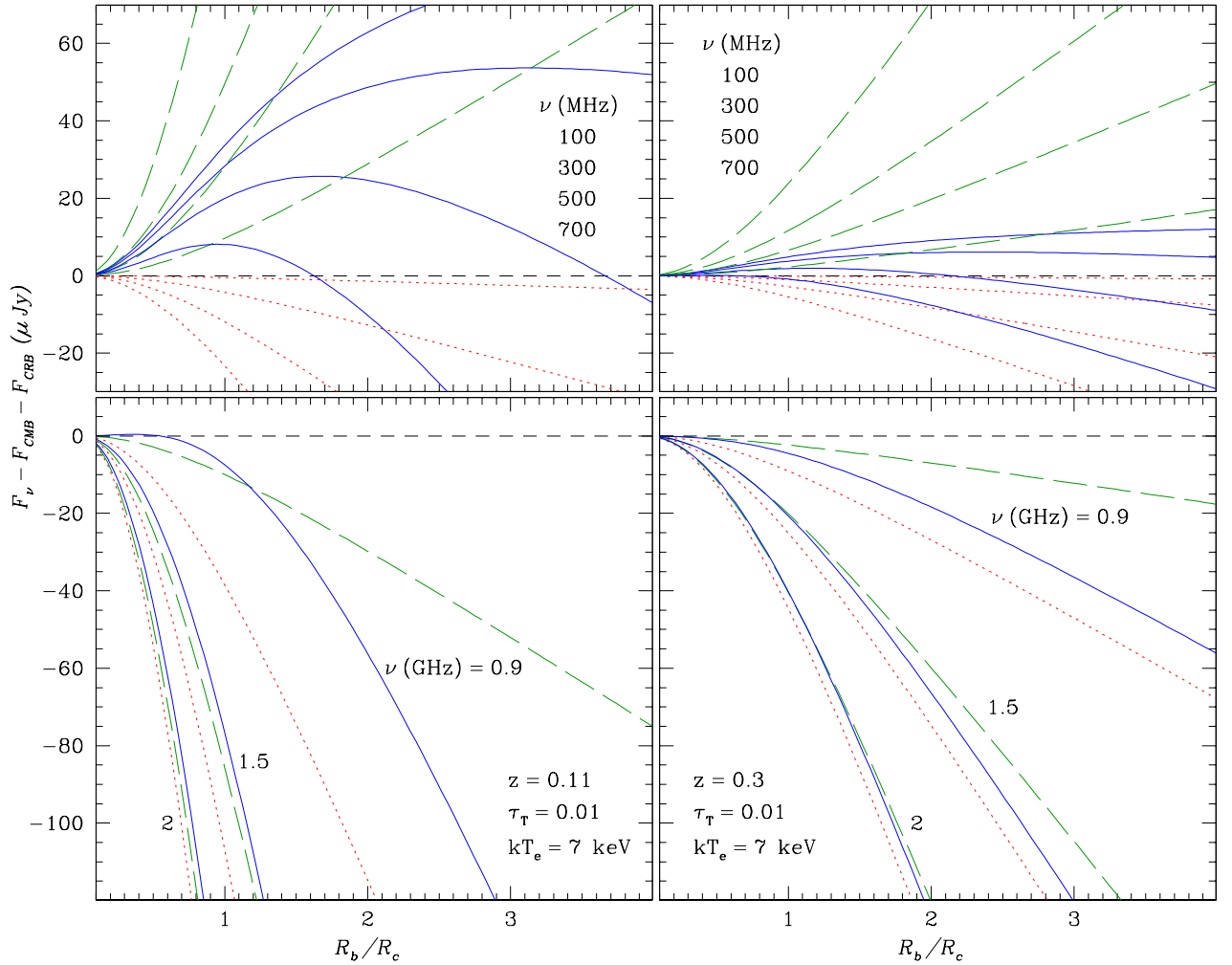


Fig. 13. The integrated radio flux within the radius R_b from a galaxy cluster with a β intergalactic gas density distribution ($\beta = 2/3$), a core radius $R_c = 350$ kpc, and a Thomson optical depth toward the center $\tau_T = 0.01$ (see Figs. 4a and 9). Such a flux will be recorded by a telescope with an angular resolution $\theta_b = R_b/d_A$, where d_A is the angular-diameter distance to the cluster. We assume the gas to be isothermal with a temperature $kT_e = 7$ keV, and the cluster itself to be at $z = 0.11$ (left) or 0.3 (right). The radio emission is associated with (1) the scattering of the cosmic radio background by electrons of the hot gas (long green dashes) or (2) the thermal bremsstrahlung of this gas (blue solid lines). In both cases, we took into account the CMB distortions due to the Compton scattering (red dotted lines). The lines of the same type correspond to different radio frequencies.

corresponding angular-diameter distances² to the cluster are $d_A \simeq 390$ or 810 Mpc; the angular size (radius) of its core is $\theta_c \simeq 3'$ or $1.5'$. Let us integrate Eqs. (11) and (12) over the cluster area $2\pi \int_0^{R_b} \rho d\rho/d_A^2$ within the solid angle limited by the half-angle $\theta_b = R_b/d_A$ to find the integrated bremsstrahlung and Compton parameters of the cluster:

$$Y_B(R_b) = 1.18 \pi^2 N_c^2 R_c \left(\frac{R_c}{d_A} \right)^2 \left[1 - \left(1 + \frac{R_b^2}{R_c^2} \right)^{-1/2} \right]$$

²We adopted the standard Λ CDM cosmological model with $\Omega_M = 0.3$, $\Omega_\Lambda = 0.7$, and $H = 70$ km s⁻¹Mpc⁻¹.

and

$$Y_C(R_b) = 2\pi\tau_T \left(\frac{kT_e}{m_e c^2} \right) \left(\frac{R_c}{d_A} \right)^2 \left[\left(1 + \frac{R_b^2}{R_c^2} \right)^{1/2} - 1 \right].$$

In particular, it can be seen that even at $R_b = 0.8 R_c$ the ratio of the integrated Compton parameter $Y_C \simeq 0.44 y_C(0)(\pi\theta_c^2)$ to the integrated bremsstrahlung parameter of the cluster $Y_B \simeq 0.21 y_B(0)(\pi\theta_c^2)$ is a factor of 2.1 greater than the ratio of their local values $y_C(0)/y_B(0)$ toward the cluster center. The bremsstrahlung, $y_B(0)$, and Compton, $y_C(0)$, parameters toward the cluster center can be found from Eqs. (11) and (12).

The actual ratio of the integrated fluxes for the radio emission that is associated with the Compton scattering of the background or is the intrinsic bremsstrahlung of the hot gas depends on the radio frequency at which the measurements are carried out. Figure 13 shows how the integrated radio flux from the galaxy cluster under consideration is gained at various frequencies as R_b increases (as the angular resolution of the telescope used for the observations degrades). The telescope is assumed to be pointed to the cluster center; the half-width of its point spread function is $\theta_b = R_b/d_A$. The left and right panels in the figure show the cases where the cluster is located at $z = 0.11$ and $z = 0.3$, respectively; the other cluster parameters and the intergalactic gas parameters were taken to be the same as those in Figs. 4a and 9.

Irrespective of the nature of the radiation, the presented fluxes take into account the scattering of CMB photons in the hot intergalactic gas (its contribution is indicated by the red dotted line). The drop in the recorded bremsstrahlung flux (and at high frequencies also the scattered radio background flux) as the angular resolution of the telescope degrades is associated precisely with the contribution of the CMB deficit. At low frequencies the scattered flux, on the contrary, increases with degrading resolution, particularly dramatically when observing a more nearby cluster. The point is that (1) the contribution of the CMB at these frequencies drops rapidly and (2) the figure presents the flux integrated over the cluster area, while the integration angle increases with increasing ratio R_b/R_c and decreasing z .

It follows from the figure that in nearby clusters (at $z \lesssim 0.11$) at low frequencies $\nu \lesssim 500$ MHz the contribution of the Compton scattering of the radio background dominates over the thermal gas radiation irrespective of the telescope's resolution. At frequencies $500 \text{ MHz} \lesssim \nu \lesssim 1 \text{ GHz}$ the Compton scattering prevails only if the point spread function of the telescope covers an extended region of the cluster ($R_b \gtrsim 1.5 - 2 R_c$). The reason is that the bremsstrahlung flux at these frequencies, after a slight initial growth, then decreases with increasing R_b , whereas the contribution of the scattering changes monotonically with increasing R_b . At frequencies $\nu \gtrsim 1 \text{ GHz}$ the thermal gas radiation makes a major contribution to the measured radio flux (an excess relative to the decrease in CMB brightness associated with its scattering), since the radio background weakens.

At the same time, in distant clusters ($z \gtrsim 0.3$) the Compton scattering of the radio background dominates over the thermal gas radiation at all of the frequencies considered up to $\nu \sim 2 \text{ GHz}$.

RADIO EMISSION FROM CLUSTER GALAXIES

Cluster galaxies often possess a powerful radio emission that can have a complex morphology (see, e.g., Hill and Longair 1971; Cuciti et al. 2018) associated with the interaction of the relativistic jets outflowing from the

galaxies and expanding plasma bubbles with the surrounding intergalactic gas, the acceleration and ejection of relativistic particles into the surrounding medium, and the generation of synchrotron radiation by them. Irregularities in the radio emission distribution are most typical for interacting, colliding galaxy clusters; they primarily manifest themselves near the shocks and contact discontinuities arising in this case.

The nonuniformity of the distribution of the synchrotron radio emission from clusters can be used for the estimation of its intensity and the proper subtraction. Similarly, if the cluster galaxies continue to remain active in the radio band at the time of their observations, then their contribution to the increase in the radio background flux observed toward the cluster can be estimated and taken into account.

An echo of the past activity of radio galaxies. The situation is different if one or more cluster galaxies were active in the past and are now in the “off” or “radio-quiet” states. Their radio emission at the epoch of activity scattered in the hot cluster gas can be observed as diffuse cluster radiation even now, leading to an additional increase in its brightness relative to the background level. The point is that the scattered emission traverses a much longer path inside the cluster than does the direct radiation from the galaxies and comes to us with a noticeable time delay due to the large cluster sizes (hundreds of parsecs). Besides, it is distributed more uniformly over the intergalactic gas cloud than is the direct radiation from the galaxies. Having a synchrotron nature, this emission is described by a power-law spectrum close to the radio background spectrum. As a result of all these factors, the scattered emission of the past activity of galaxies can make it much more difficult to detect and identify the excess of the radio background associated with its scattering in the hot cluster gas.

In contrast to the Compton scattering of the isotropic background radiation whose distortions arise due to the relativistic (Doppler) effects $\sim kT_e/mc_e^2$, the diffuse radiation from active galaxies is determined mainly by the change in the direction of photon motion upon Thomson scattering. The change in the photon frequency upon scattering affects the spectrum of the diffuse radiation insignificantly (at the same level $\sim kT_e/mc_e^2 \sim 1-2\%$, see Eq. [4]).

If an active galaxy is at the cluster center and switched off only recently, $t_{so} \ll R_c/c$, while before this it shined for a long time in the radio band at approximately the same level and had a power-law spectrum with a spectral index γ , then the integrated, direction-averaged, spectral density of the scattered emission from the cluster can be easily calculated:

$$F_\nu(\nu) = F_A(\nu)\tau_c R_c^2/d_L^2, \text{ where} \quad (13)$$

$$F_A(\nu) = \frac{L_R}{4\pi R_c^2} \left(\frac{(1-\gamma) 10^{14}}{10^{(2-2\gamma)} - 10^{(2\gamma-2)}} \right) \nu_9^{-\gamma} \text{ Jy.} \quad (14)$$

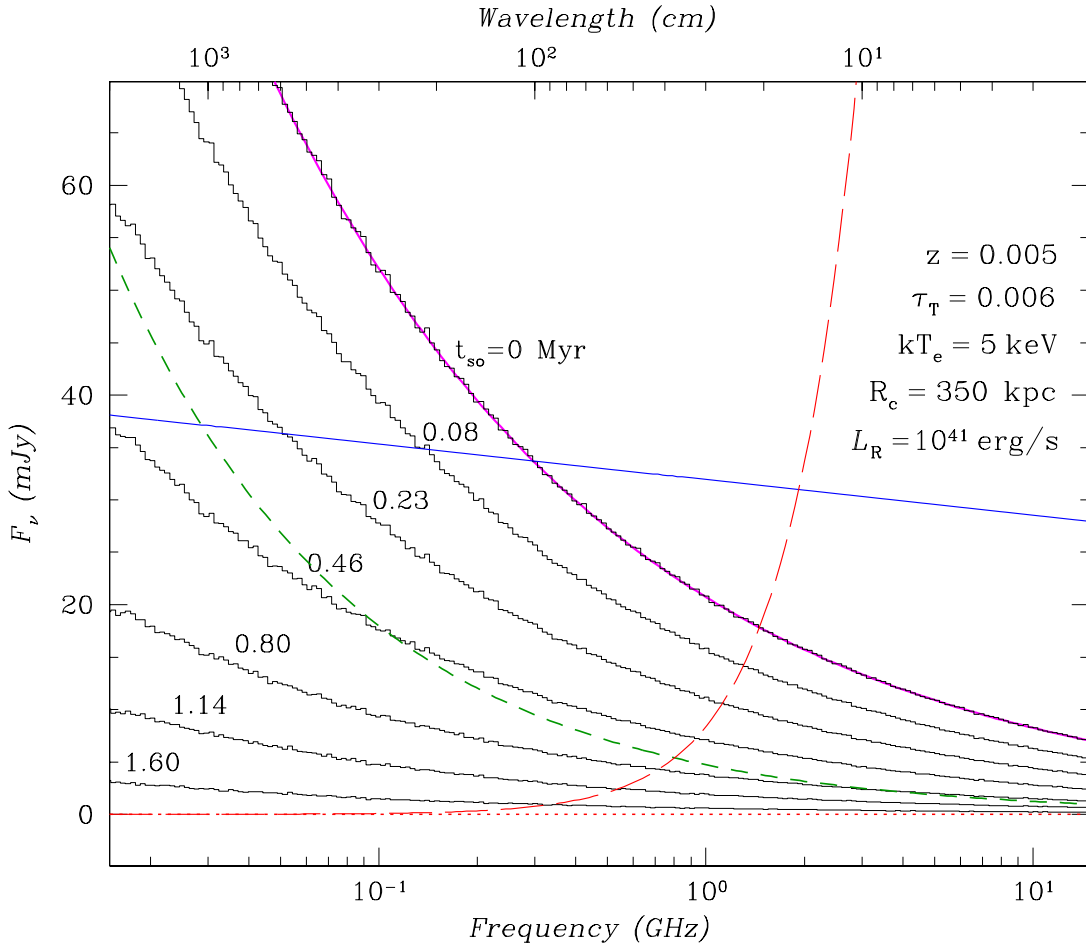


Fig. 14. The distortions in the spectrum of the cosmic radio background due to its scattering by electrons of the hot cluster gas (green dashes), the bremsstrahlung of this gas (blue solid line), and the scattered (diffuse) radiation of the central galaxy (histograms). The red curve (long dashes) indicates the absolute value of the decrease in CMB brightness due to its scattering in the cluster gas. The integrated flux (from the entire cluster) is presented everywhere. It is assumed that the galaxy had been active for a long time in the radio band with a spectral index $\gamma = 0.4$ and a luminosity $L_R = 1 \times 10^{41} \text{ erg s}^{-1}$ in the frequency range 10 MHz – 100 GHz, but switched off t_{so} million years ago. The histograms are obtained from Monte Carlo computations. The case of $t_{\text{so}} = 0$ was also calculated analytically (Eq. [13], the dark-red line). We consider a nearby ($z = 0.005$) cluster with a uniform isothermal ($kT_e = 5 \text{ keV}$) gas density, a radius $R_c = 350 \text{ kpc}$, and an optical depth along the line of sight $\tau_T = 0.006$ (the same as that in Fig. 2).

Here, ν_9 is the frequency in GHz, L_R is the radio luminosity of the galaxy in erg s^{-1} in the range 10 MHz – 100 GHz before the switch-off, and $d_L(z)$ is the luminosity distance at which it is located.

Figure 14 presents the results of such calculations performed under the assumption that $\gamma = 0.4$, $L_R = 1 \times 10^{41} \text{ erg s}^{-1}$, and the galaxy cluster is at $z = 0.005$, i.e., at a luminosity distance $d_L = 21.44 \text{ Mpc}$ (an angular-diameter distance $d_A = 21.23 \text{ Mpc}$). The cluster radius $R_c = 350 \text{ kpc}$ corresponds to an angular size $\theta_c = 57'$; the electron density distribution is assumed to be uniform. The remaining cluster parameters were taken to be the same as those in Fig. 2. The model cluster with such parameters resembles the Virgo cluster, but con-

tains a hotter gas.

The result of our calculation using Eq. (13) is indicated by the dark-red line. The histograms represent the results of analogous Monte Carlo computations using the algorithms of Pozdnyakov et al. (1983). We used the computer code developed by us when working on our previous paper (Grebenev and Sunyaev 2019). The analytical curve is seen to agree excellently with our numerical computation for the galaxy switch-off at $t_{\text{so}} = 0$. Other histograms indicate the spectrum of the diffuse radiation that must be recorded from the cluster a certain time, $t_{\text{so}} = 0.08, 0.23, 0.46, 0.80, 1.14,$ and 1.60 Myr , after its switch-off. Note that the last photon of the intrinsic (direct) radiation from the galaxy

leaves the hot-gas cloud in the cluster $R_c/c \simeq 1.14$ Myr after its switch-off. We must record the spectrum at precisely this time. The scattered photons of the last two histograms spent more than twice as long in the cloud.

Figure 14 also presents the spectral density of the thermal (bremsstrahlung) radiation from the hot ($kT_e = 5$ keV) cluster gas (blue solid line) and the excess radiation associated with the Compton scattering of the radio background (green dashes). In contrast to most of the previous figures, the fluxes from the entire cluster obtained by the integration over its apparent solid angle $2\pi \int_0^{R_c} \rho d\rho/d_A^2$ are presented here. Also, in contrast to other figures, here we ignored the decrease in CMB brightness. Instead, the absolute value of this decrease is shown (long red dashes). Clearly, at frequencies above $\sim 1 - 1.5$ GHz all of the excess radiation associated with the past activity of the galaxy, along with the radiation associated with the radio background scattering and the cluster gas bremsstrahlung, are completely suppressed by the decrease in CMB brightness. At the same time, at frequencies $\nu \lesssim 300$ MHz the diffuse radiation from the recently ($\lesssim 0.5$ Myr ago) switched-off galaxy with the above luminosity can dominate in the radio background excess being detected toward the cluster, exceeding both the background scattering effect and the contribution of the thermal gas radiation. In the frequency range $300 \text{ MHz} \lesssim \nu \lesssim 1.5 \text{ GHz}$ the thermal intergalactic gas radiation dominates in the cluster with the chosen parameters.

Figure 14 shows that the scattered emission from the cluster galaxy that was active in the past may turn out to be a serious obstacle in the way of detecting (to be more precise, identifying) the excess of the radio background associated with its Compton scattering by electrons of the hot intergalactic gas in this direction. Of course, the case considered suggests that the galaxy was very bright in the radio range in the recent past. However, for a massive central cluster galaxy such activity cannot be ruled out.

The fact that the diffuse radiation in distant clusters at high redshifts z must be greatly attenuated compared to the scattered background radiation (independent of z) causes some optimism. Above we showed how rapidly the intensity of the thermal radiation from the hot cluster gas decreases with increasing z . The problem is that the spectra of the scattered background radiation and the diffuse radiation from an active galaxy are very close in shape (dependence on ν) and they are difficult to distinguish.

Morphology of the diffuse radiation from a radio galaxy.

Certain hopes for revealing the scattered background radiation can be associated with different morphologies of the distribution of its brightness and the brightness of the diffuse radiation from a switched-off galaxy in the picture plane of the cluster. Indeed, when observing a cluster with a uniform hot-gas density distribution using

an antenna with a good angular resolution ($\ll R_c/d_A$, where d_A is the angular-diameter distance to the cluster), the background excess flux, along with the intensity of the thermal gas radiation, depend on the impact parameter ρ proportionally to $(1 - \rho^2/R_c^2)^{1/2}$. The situation is different for the scattered emission from a radio galaxy that switched off only recently.

Although the integrated scattered flux is gained with radius (to be more precise, with radial optical depth, see Eq. [13]) linearly (the fraction of the emission scattered in a spherical layer at a given radius is determined only by its optical depth $\Delta \tau_T$), the intensity of the scattered emission obtained by the integration along the line of sight at an impact parameter ρ depends on ρ in a more complicated way:

$$F_\nu(\nu) = F_A(\nu) \frac{\tau_T R_c}{4\pi\rho} \arctg \sqrt{R_c^2/\rho^2 - 1}, \quad (15)$$

where the flux $F_A(\nu)$ is defined by Eq. (14). The results of our calculations of the radio excess toward a galaxy cluster (in comparison with the background level) associated with the scattered emission of a switched-off central galaxy using this formula are shown in Fig. 15 as a function of ρ for several radio frequencies (black dotted lines). It can be seen that this emission is characterized by a powerful central peak that is narrower at high frequencies $\nu \gtrsim 1$ GHz and broader at low ones $\nu \lesssim 500$ MHz. It follows from Eq. (15) that the frequency dependence reflects simply the power of the emission from the galaxy at a given frequency. The distribution of other excess radiation components also shown in the figure, namely the bremsstrahlung (blue dashes), the scattered radio background (cyan solid lines), and the missing CMB due to the scattering (long red dashes), is much flatter and smoother. All of the components, except for the diffuse radiation from the galaxy, are measured from the CMB decrement. The green solid lines indicate the distribution of the combined excess radiation. Remarkably, the central peak is retained at all frequencies and can be used to reveal the scattered emission from a recently switched-off central cluster galaxy (or to prove the absence of this emission). The central emission peak is also retained in the case where the galaxy switched off a longer time ago. In this case, however, its amplitude decreases; moreover, near the cluster center the intensity of the scattered emission drops sharply. This is because the photons of the direct radiation from the galaxy leave this region and can no longer be involved in the scattering. Obviously, the angular radius of this region of a reduced diffuse background is $\theta_0 \sim ct_{so}/d_A$. Undoubtedly, the detected peculiarities of the diffuse radiation morphology in the cluster are also retained for a more realistic hot-gas density distribution than the uniform distribution considered.

Note also that, as is obvious from Fig. 15, the diffuse radiation from a recently switched-off powerful central active galaxy must maintain (and enhance) the hybrid

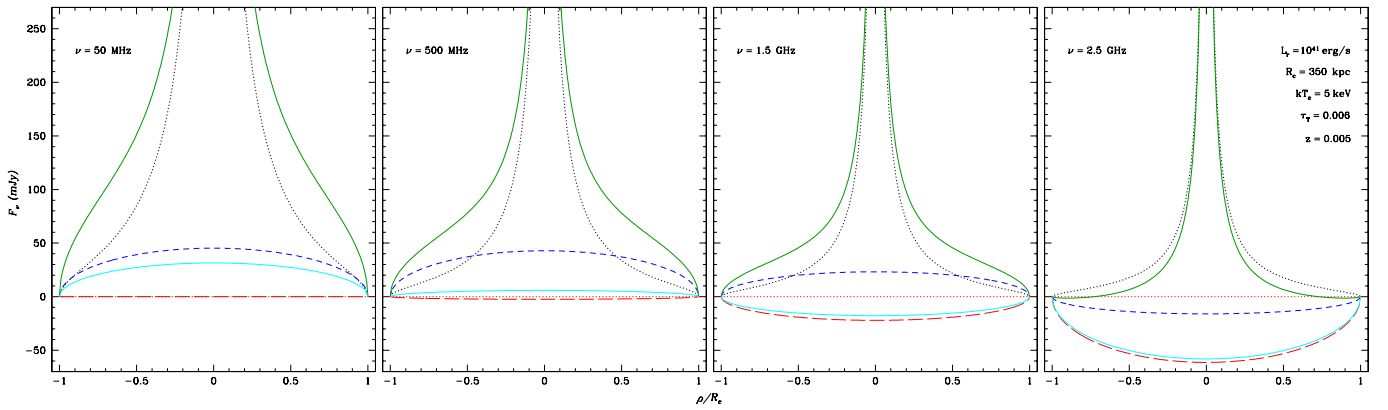


Fig. 15. Cosmic radio background excess toward a galaxy cluster versus impact parameter ρ (green solid line). The cyan solid line indicates the distortions due to the scattering in the hot cluster gas, the short blue dashes indicate the contribution of the gas bremsstrahlung, and the black dotted line indicates the scattered emission from the central galaxy. Everywhere, except for the galaxy emission, we took into account the decrease in the brightness of the CMB due to its Compton scattering (long red dashes). It is assumed that the galaxy was active for a long time and had a spectral index $\gamma = 0.4$ and a luminosity $L_R = 1 \times 10^{41} \text{ erg s}^{-1}$ in the range 10 MHz – 100 GHz, but recently ($t_{\text{so}} \simeq 0$) it switched off. The cluster is considered with the same parameters as those in Fig. 14.

shape of the brightness distribution of the radio source toward the cluster discussed above in this paper.

Induced scattering of the emission from a galaxy. Above (Fig. 2) we showed that the radio background distortions due to the induced Compton scattering manifest themselves only at very low frequencies $\nu \lesssim 5$ MHz. When the emission from a powerful radio galaxy is scattered in the cluster gas, the induced scattering can increase noticeably in importance. This is because the intensities of the emission in the immediate vicinity of the galaxy are high. Therefore, in particular, the question about the possibility of gas heating near active galactic nuclei and quasars to quasi-relativistic temperatures through the induced Compton scattering of their radio emission was actively discussed (Levich and Sunyaev 1971; Sazonov and Sunyaev 2001). The distortions in the spectrum of a radio source due to the induced scattering were considered in Sunyaev (1970).

Acting in the same way as in the derivation of Eq. (5) and again using Eq. (14) to determine the flux $F_A(\nu)$, we find the spectrum of the scattered emission from a recently switched-off radio galaxy:

$$F_\nu(\nu) = F_A \tau_c \frac{R_c^2}{d_L^2} \left[1 - F_A \frac{(1 + \gamma) R_c^2}{m_e 10^{23} \nu^2} \left(\frac{R_c}{R_0} - 1 \right) \right] \quad (16)$$

Here, R_0 is the radius of the region surrounding the nucleus of the radio galaxy into which the hot intergalactic gas does not penetrate and, therefore, in which no induced scattering occurs. The results of our calculations using this formula are shown in Fig. 16 for the same cluster as that in Fig. 14 under different assumptions about the galaxy luminosity $L_R = L_{41} \times 10^{41} \text{ erg s}^{-1}$, where $L_{41} = 2, 1, \text{ or } 0.4$ in the frequency range 10 MHz – 100 GHz, and the radius R_0 . It can be seen that the scat-

tered flux from the central radio galaxy drops sharply due to the induced scattering already at frequencies ~ 50 MHz and, in a number of cases, even at $\sim 100\text{--}150$ MHz, which opens the possibility of observing the scattered radio background at lower frequencies. Recall that the induced scattering reduces the contribution of the scattered radio background at much lower frequencies ($\lesssim 5$ MHz, Fig. 2).

The action of the induced scattering may turn out to be even stronger due to the scattering of the emission from a radio galaxy by electron density fluctuations in the cluster gas. This effect leads to a pulse broadening and rapid intensity scintillations of radio pulsars at low frequencies and a smearing of their images on radio maps (see, e.g., Cordes and Lazio 1991; Bhat et al. 2004). In our case, it is important that the scattering by electron density fluctuations lengthens the path of the photons emitted by the radio galaxy in the cluster gas and increases the probability of their induced scattering.

Radiation from relativistic electrons. Apart from the synchrotron radiation directly associated with the activity of cluster galaxies, the diffuse radiation (radio halo) explained by the radiation of relativistic electrons accelerated at shocks during cluster mergers or collisions is observed in some clusters (Brunetti et al. 2001; van Weeren 2019). As a rule, no radio halo is observed in relaxed clusters (Cuciti et al. 2021). The fraction of clusters with a radio halo is 20–50%, increasing with cluster mass and redshift (Cassano et al. 2023). The halo size is comparable to the size of the X-ray source at the location of the cluster, i.e., the width of the bremsstrahlung profile of the hot intergalactic gas.

The lifetime of relativistic electrons can reach 10–100 Myr, so that their radiation remains bright noticeably

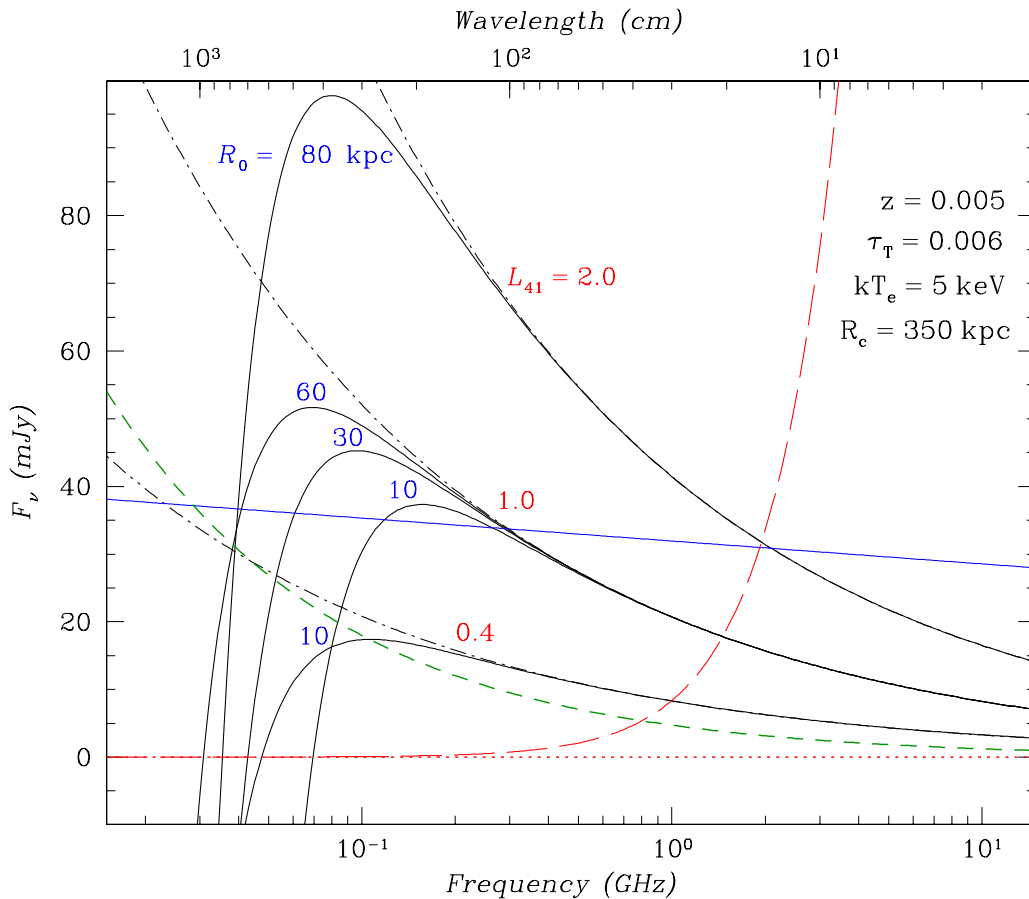


Fig. 16. Same as Fig. 14, but for central galaxies of various luminosities in the frequency range 10 MHz – 100 GHz, $L_R = L_{41} \times 10^{41} \text{ erg s}^{-1}$, where $L_{41} = 2, 1, \text{ or } 0.4$ (indicated by the red numbers), that switched off only recently, $t_{\text{so}} = 0$. The radio emission from the galaxies scattered in the gas is indicated by the black dash-dotted lines. The black solid lines indicate the scattered emission from the galaxies including the induced Compton scattering. It is assumed that the scattering gas is absent within the radius $R_0 = 10 - 80 \text{ kpc}$ (blue numbers) near the galaxies.

longer than the diffuse (scattered in the cluster) radiation from galaxies. The spectral slope of the synchrotron radiation from halo electrons is almost flat at the cluster center ($\alpha \sim 0.2$) and becomes steeper ($\alpha \sim 0.5$) on the periphery (Brunetti et al. 2001).

Obviously, the synchrotron radiation from the halo can become an almost unsurmountable obstacle when investigating the radio background scattering effect in the hot cluster gas. Therefore, it makes sense to study only well-relaxed clusters or to use peripheral observations (the distortions due to the scattering must have a larger scale than the halo size). Just as the thermal bremsstrahlung flux, the nonthermal synchrotron (diffuse) flux must decrease rapidly with redshift. Therefore, it is more preferable to observe distant clusters.

CONCLUSIONS

We explored the possibility of observing the increase in the brightness of the radio background toward galaxy

clusters due to its Compton scattering by electrons of the hot intergalactic gas. At frequencies above 800 MHz this scattering leads to a decrease in the CMB brightness — an effect predicted by Sunyaev and Zeldovich (1970, 1972) and later confirmed in many ground-based and space experiments. At present, this effect is one of the main methods of observational cosmology (along with direct X-ray and optical observations and gravitational lensing methods). In contrast to direct observations, this effect does not depend on the distance, allowing clusters at high redshifts to be investigated.

In recent years, as new highly sensitive radio telescopes are put into operation, it has been possible to also measure the spectrum of the cosmic radio background with a high accuracy at frequencies from tens of MHz to several GHz. It probably has a synchrotron origin (a power-law spectrum). However, on the whole, its nature is unclear; it is possible to associate no more than 25% of the measured flux with faint unresolved radio galaxies. Nevertheless, the radio background has a

high degree of isotropy and homogeneity like the CMB. The relevant question has arisen as to whether the radio background distortions can be observed towards galaxy clusters due to its interaction with the hot intergalactic gas. Observations of the distortions would allow one to investigate both the galaxy clusters and the properties of the radio background at high redshifts proper.

As a result of our computations, we showed the following.

(1) The effect does exist, and at frequencies $\nu \lesssim 800$ MHz the excess of the radio flux above the background that is formed due to the scattering must more than compensate for the CMB deficit.

(2) The excess of radiation again disappears at frequencies $\nu \lesssim 5$ MHz due to the action of the induced Compton scattering that carries away the photons downward along the frequency axis.

(3) In many cases, the intrinsic thermal (bremsstrahlung) radiation of the hot intergalactic gas and, possibly, the scattered synchrotron radiation associated either with the past activity of cluster galaxies in the radio band (the contribution of their radiation at the current level of activity can still be taken into account and removed) or with the radiation of relativistic electrons produced in shocks when a given cluster merges or tidally interacts with its nearest neighbors must hinder the direct measurement of the Compton excess of radiation.

(4) The contribution of both bremsstrahlung and synchrotron radiation must decrease rapidly as the cluster recedes (as its redshift increases).

(5) In many nearby clusters the bremsstrahlung of the hot gas completely dominates at frequencies from 10–50 MHz to 2–6 GHz; the frequency ranges optimal for searching for and measuring the Compton excess of the radio background flux were determined for various parameters of clusters. Massive clusters with a hot ($kT_e \gtrsim 8$ keV) rarefied ($N_e \lesssim 10^{-2} \text{ cm}^{-3}$) intergalactic gas at high ($z \gtrsim 0.5$) redshifts turned out to be most promising for such observations.

(6) The peripheral observations of rich unperturbed clusters with a density distribution that gradually falls off with radius have certain advantages for detecting the Compton excess of the radio background (because of the faster drop in the radio bremsstrahlung flux).

(7) The cluster image on the radio background maps in the frequency range 1.0–1.5 GHz must take a highly unusual (“hybrid”) form — a bright source at the center (associated with the excess bremsstrahlung) surrounded by a ringlike shadow region (a region of the CMB deficit due to the scattering); at lower frequencies the source toward the cluster has a usual (“positive”) form initially because of the increase in bremsstrahlung intensity and subsequently because of the excess of the radio background due to its scattering in the cluster gas; at higher frequencies a shadow (“negative”) source (a “hole” in the background) appears at the location of the cluster

because of the CMB deficit associated with to the scattering by electrons.

(8) The transition near a frequency of 217 GHz from the “negative” source on the maps of CMB fluctuations (due to the upward escape of photons along the frequency axis upon their scattering in the cluster gas) to the “positive” one (because of the scattered photons coming to the region $\nu > 217$ GHz) is also accompanied by the appearance of a “hybrid” source at the location of the cluster with a bright peak of bremsstrahlung rising from the center of a wide Compton hole.

(9) The presence of radio galaxies in the cluster that were active in the past can additionally complicate the observations of the excess of the radio background due to its Compton scattering: their synchrotron radiation scattered in the intergalactic gas traverses a noticeably longer path (because of the giant cluster sizes — hundreds of parsecs) and arrives with a noticeable delay; it is the scattered radiation that is important, since the contribution of the current radiation from galaxies to the total radio flux from the cluster can still be calculated and taken into account; the scattered radiation has a synchrotron nature and a power-law spectrum close to the background spectrum.

(10) It is possible to measure the excess of the radio background associated with the scattering if the luminosity of the cluster radio galaxies and the time elapsed after their switch-off satisfy certain constraints; we estimated them by using the Monte Carlo method; we also showed that the diffuse radiation of galaxies is suppressed due to the induced Compton scattering at $\nu \lesssim 50 - 100$ MHz, which opens the possibility of observing the scattered radiation of the cosmic radio background at these frequencies without obstruction.

(11) The morphology of the scattered radiation from radio galaxies differs greatly both from the flat distribution of the scattered radio background and from the distribution of the bremsstrahlung from the hot cluster gas; this can be used to identify the radio excess detected toward the cluster.

In conclusion, note that the diffuse synchrotron radiation from the relativistic electrons in the cluster gas probably formed during the merging or the tidal effect on the cluster from its neighbors observed as a giant radio halo can be the most serious obstacle in the way of detecting and identifying the Compton excess of the radio background. To detect the excess, it is necessary to use well-relaxed clusters in which, as a rule, no radio halo is observed and, desirably, clusters at sufficiently high redshifts, since the intensity of the synchrotron radiation drops rapidly with z .

ACKNOWLEDGMENTS

We thank S.A. Trushkin and E.M. Churazov for their useful remarks.

FUNDING

The participation of S.A. Grebenev was supported by the BASIS Foundation for the Advancement of Theoretical Physics and Mathematics, grant no. 22-1-1-57-1 of the Program “Leading Scientist (Theoretical Physics)”.

CONFLICT OF INTEREST

The authors of this work declare that they have no conflicts of interest.

REFERENCES

1. K. Abazajian, G. Addison, P. Adshead, Z. Ahmed, S. W. Allen, D. Alonso, M. Alvarez, A. Anderson, et al., arXiv:1907.04473 (2019).
2. P. A. R. Ade, N. Agranim, C. Armitage-Caplan, M. Arnaud, M. Ashdown, F. Atrio-Barandela, J. Aumont, H. Aussel, et al. (Planck Collaboration), *Astron. Astrophys.* **571**, id. A29 (2014).
3. P. A. R. Ade, N. Agranim, C. Armitage-Caplan, M. Arnaud, M. Ashdown, F. Atrio-Barandela, J. Aumont, H. Aussel, et al. (Planck Collaboration), *Astron. Astrophys.* **581**, id. A14 (2015).
4. P. A. R. Ade, N. Agranim, M. Arnaud, M. Ashdown, J. Aumont, C. Baccigalupi, A. J. Banday, R.B. Barreiro, et al. (Planck Collaboration), *Astron. Astrophys.* **594**, id. A27 (2016).
5. P. Ade, J. Aguirre, Z. Ahmed, S. Aiola, A. Ali, D. Alonso, M. A. Alvarez, K. Arnold, et al., *J. Cosm. Astropart. Phys.* **02**, 056 (2019).
6. M. Amiri, K. M. Bandura, P. J. Boyle, C. Brar, J.-F. Cliche, K. Crowter, D. Cubranic, P. B. Demorest, et al. (CHIME/Pulsar Collab.), *Astrophys. J. Suppl. Ser.* **255**, 5 (2021).
7. M. Arnaud, *Astron. Astrophys.* **500**, 103 (2009).
8. D. J. Bacon, R. A. Battye, P. Bull, S. Camera, P. G. Ferreira, I. Harrison, D. Parkinson, A. Pourtsidou, et al. (Square Kilometre Array Cosmol. Sci. Working Group), *Publ. Astron. Soc. Austral.* **37**, 7 (2020).
9. N.D.R. Bhat, J.M. Cordes, F. Camilo, D.J. Nice, and D.R. Lorimer, *Astrophys. J.* **605**, 759 (2004).
10. M. Birkinshaw, *Phys. Rep.* **310**, 97 (1999).
11. L. E. Bleem, B. Stalder, T. de Haan, K. A. Aird, S. W. Allen, D. E. Applegate, M. L. N. Ashby, M. Bautz, et al., *Astrophys. J. Suppl. Ser.* **216**, 27 (2015).
12. L. E. Bleem, S. Bocquet, B. Stalder, M. D. Gladders, P. A. R. Ade, S. W. Allen, A. J. Anderson, J. Annis, et al., *Astrophys. J. Suppl. Ser.* **247**, 25 (2020).
13. G. Brunetti, G. Setti, L. Feretti, and G. Giovannini, *Mon. Not. Roy. Astron. Soc.* **320**, 365 (2001).
14. A. G. W. Cameron, in “*Essays in Nuclear Astrophysics. Presented to William A. Fowler*” (eds. C. A. Barnes, D. D. Clayton, D. N. Schramm; Cambridge Univ. Press, Cambridge, 1982), p. 23.
15. J. E. Carlstrom, G. P. Reese, and D. Erik, *Ann. Rev. Astron. Astrophys.* **40**, 643 (2002).
16. R. Cassano, V. Cuciti, G. Brunetti, A. Botteon, M. Rossetti, L. Bruno, A. Simionescu, F. Gastaldello, et al., *Astron. Astrophys.* **672**, A43 (2023).
17. A. Cavaliere and R. Fusco-Femiano, *Astron. Astrophys.* **49**, 137 (1976).
18. J. J. Condon, W. D. Cotton, E. B. Fomalont, K. I. Kellermann, N. Miller, R. A. Perley, D. Scott, T. Vernstrom, and J. V. Wall, *Astrophys. J.* **758**, 23 (2012).
19. A. Cooray, *Phys. Rev. D* **73**, 103001 (2006).
20. J. M. Cordes and T. J. Lazio, *Astrophys. J.* **376**, 123 (1991).
21. V. Cuciti, G. Brunetti, R. van Weeren, A. Bonafede, D. Dallacasa, R. Cassano, T. Venturi, and R. Kale, *Astron. Astrophys.* **609**, A61 (2018).
22. V. Cuciti, R. Cassano, G. Brunetti, D. Dallacasa, R.J. van Weeren, S. Giacintucci, A. Bonafede, F. de Gasperin, et al., *Astron. Astrophys.* **647**, A50 (2021).
23. K. S. Dawson, W. L. Holzapfel, J. E. Carlstrom, M. Joy, S. J. LaRoque, A. D. Miller, and D. Nagai, *Astrophys. J.* **581**, 86 (2002).
24. J. Dowell and G. B. Taylor, *Astrophys. J.* **858**, L9 (2018).
25. D. J. Fixsen, A. Kogut, S. Levin, M. Limon, P. Lubin, P. Mirel, M. Seiffert, J. Singal, et al., *Astrophys. J.* **734**, 5 (2011).
26. S. A. Grebenev and R. A. Sunyaev, *Astron. Lett.* **45**, 791 (2019).
27. S. A. Grebenev and R. A. Sunyaev, *J. Cosm. Astropart. Phys.* submitted (2024).
28. T. de Haan, B. A. Benson, L. E. Bleem, S. W. Allen, D. E. Applegate, M. L. N. Ashby, M. Bautz, M. Bayliss, et al., *Astrophys. J.* **832**, 95 (2016).
29. M. P. van Haarlem, M. W. Wise, A. W. Gunst, G. Heald, J. P. McKean, J. W. T. Hessels, A. G. de Bruyn, R. Nijboer, et al., *Astron. Astrophys.* **556**, A2 (2013).
30. M. J. Hardcastle, T. W. Shimwell, C. Tasse, P. N. Best, A. Drabent, M. J. Jarvis, I. Prandoni, H. J. A. Röttgering, et al., *Astron. Astrophys.* **648**, 10 (2021).
31. M. Hasselfield, M. Hilton, T. A. Marriage, G. E. Addison, L. F. Barrientos, N. Battaglia, E. S. Battistelli, J.R. Bond, et al., *J. Cosm. Astropart. Phys.* **07**, 008 (2013).
32. J. M. Hill and M. S. Longair, *Mon. Not. Roy. Astron. Soc.* **154**, 125 (1971).
33. M. Hilton, C. Sifon, S. Naess, M. Madhavacheril, M. Oguri, E. Rozo, E. Rykoff, T. M. C. Abbott, et al., *Astrophys. J. Suppl. Ser.* **253**, 3 (2021).
34. G. P. Holder and J. Chluba, *Astrophys. J.* arXiv:2110.08373 (2021).
35. A. W. Hotan, J. D. Bunton, A. P. Chippendale, M. Whiting, J. Tuthill, V. A. Moss, D. McConnell, S. W. Amy, et al., *Publ. Astron. Soc. Austral.* **38**, 9 (2021).
36. J. Jonas and MeerKAT Team, in *Proc. “MeerKAT Sci-*

- ence: *On the Pathway to the SKA*” (Stellenbosch, South Africa), p. 1 (2016).
37. C. Jones and W. Forman, *Astrophys. J.* **276**, 38 (1984).
 38. A. S. Kompaneets, *Sov. Phys. JETP* **4**, 730 (1957).
 39. K. R. Lang, “*Astrophysical formulae (A Compendium for the Physicist and Astrophysicist)*”, (Springer-Verlag, Berlin, 1974).
 40. E. Lee, J. Chluba, and G. P. Holder, *Mon. Not. Roy. Astron. Soc.* **512**, 5153 (2022).
 41. E. V. Levich and R. A. Sunyaev, *Sov. Astron.* **15**, 363 (1971).
 42. K. Maeda, H. Alvarez, J. Aparici, J. May, and P. Reich, *Astron. Astrophys. Suppl. Ser.* **140**, 145 (1999).
 43. L. Di Mascolo, Ph.D. Thesis, Ludwig Maximilian University (2020).
 44. T. Mroczkowski, D. Nagai, K. Basu, J. Chluba, J. Sayers, R. Adam, E. Churazov, A. Crites, et al., *Space Sci. Rev.* **215**, 17 (2019).
 45. L. A. Pozdnyakov, I. M. Sobol’, and R. A. Sunyaev, *Sov. Sci. Rev., Sec. E: Astrophys. Space Phys. Rev.* **2**, 189 (1983).
 46. P. Reich, J. C. Testori, and W. Reich, *Astron. Astrophys.* **376**, 861 (2001).
 47. M. Remazeilles, C. Dickinson, A. J. Banday, M.-A. Bigot-Sazy, and T. Ghosh, *Mon. Not. Roy. Astron. Soc.* **451**, 4311 (2015).
 48. R. S. Roger, C. H. Costain, T. L. Landecker, and C. M. Swerdlyk, *Astron. Astrophys.* **137**, 7 (1999).
 49. A. Sabyr, J. C. Hill, and B. Boliet, *Phys. Rev. D* **106**, 023529 (2022).
 50. S. Yu. Sazonov and R. A. Sunyaev, *Astron. Lett.* **27**, 481 (2001).
 51. N. Sehgal, S. Aiola, Y. Akrami, K. Basu, M. Boylan-Kolchin, S. Bryan, C. M. Casey, S. Clesse, et al., *BAAS* **51**, 6 (2019).
 52. M. Seiffert, D. J. Fixsen, A. Kogut, S. M. Levin, M. Limon, P. M. Lubin, P. Mirel, J. Singal, et al., *Astrophys. J.* **734**, 6 (2011).
 53. J. Singal, N. Fornengo, M. Regis, G. Bernardi, D. Bordenave, E. Branchini, N. Cappelluti, A. Caputo, et al., *PASP* **135**, 1045, id.036001 [arXiv:2211.16547] (2023).
 54. R. A. Sunyaev, *Astrophys. Lett.* **7**, 19 (1970).
 55. R. A. Sunyaev, *Sov. Astron. Lett.* **6**, 213 (1980).
 56. R. A. Sunyaev and Ya. B. Zeldovich, *Astrophys. Sp. Sci.* **7**, 3 (1970).
 57. R. A. Sunyaev and Ya. B. Zeldovich, *Comm. Astrophys. Sp. Phys.* **4**, 173 (1972).
 58. R. A. Sunyaev and Ya. B. Zeldovich, *Ann. Rev. Astron. Astrophys.* **18**, 537 (1980).
 59. R. A. Sunyaev and Ya. B. Zeldovich, *Sov. Sci. Rev., Sec. E: Astrophys. Space Phys. Rev.* **1**, 1 (1981).
 60. T. Venturi, S. Giacintucci, D. Dallacasa, R. Cassano, G. Brunetti, S. Bardelli, and G. Setti, *Astron. Astrophys.* **484**, 327 (2008).
 61. R. J. van Weeren, F. de Gasperin, H. Akamatsu, M. Brüggén, L. Feretti, H. Kang, A. Stroe, F. Zandanel, *Space Sci. Rev.* **215**, 16 (2019).
 62. R. Williamson, B. A. Benson, F. W. High, K. Vanderlinde, P. A. R. Ade, K. A. Aird, K. Andersson, R. Armstrong, et al., *Astrophys. J.* **738**, 139 (2011).
 63. F. Wu, J. Li, S. Zuo, X. Chen, S. Das, J. P. Marriner, T. M. Oxholm, A. Phan, et al., *Mon. Not. Roy. Astron. Soc.* **506**, 3455 (2021).
 64. Ya. B. Zeldovich and I. D. Novikov, “*Relativistic Astrophysics, Vol. 2: The Structure and Evolution of the Universe*” (Nauka, Moscow, 1975; Univ. Chicago Press 1983).
 65. Ya. B. Zeldovich and R. A. Sunyaev, in “*Astrophysics and Space Physics*” (Ed. R. A. Sunyaev; Nauka, Moscow, 1982; Routledge, London, 1984), p. 9.

Translated by V. Astakhov